

# AGB stars in the SMC: evolution and dust properties based on *Spitzer* observations

F. Dell’Agli,<sup>1,2★</sup> D. A. García-Hernández,<sup>3,4</sup> P. Ventura,<sup>2</sup> R. Schneider,<sup>2</sup>  
M. Di Criscienzo<sup>2</sup> and C. Rossi<sup>1</sup>

<sup>1</sup>*Dipartimento di Fisica, Università di Roma “La Sapienza”, P.le Aldo Moro 5, I-00143 Roma, Italy*

<sup>2</sup>*INAF – Osservatorio Astronomico di Roma, Via Frascati 33, I-00040 Monte Porzio Catone (RM), Italy*

<sup>3</sup>*Instituto de Astrofísica de Canarias, C/ Via Láctea s/n, E-38205 La Laguna, Tenerife, Spain*

<sup>4</sup>*Departamento de Astrofísica, Universidad de La Laguna (ULL), E-38206 La Laguna, Tenerife, Spain*

Accepted 2015 October 1. Received 2015 October 1; in original form 2015 July 28

## ABSTRACT

We study the population of asymptotic giant branch (AGB) stars in the Small Magellanic Cloud (SMC) by means of full evolutionary models of stars of mass  $1 M_{\odot} \leq M \leq 8 M_{\odot}$ , evolved through the thermally pulsing phase. The models also account for dust production in the circumstellar envelope. We compare *Spitzer* infrared colours with results from theoretical modelling. We show that  $\sim 75$  per cent of the AGB population of the SMC is composed by scarcely obscured objects, mainly stars of mass  $M \leq 2 M_{\odot}$  at various metallicity, formed between 700 Myr and 5 Gyr ago;  $\sim 70$  per cent of these sources are oxygen-rich stars, while  $\sim 30$  per cent are C-stars. The sample of the most obscured AGB stars, accounting for  $\sim 25$  per cent of the total sample, is composed almost entirely by carbon stars. The distribution in the colour–colour ( $[3.6] - [4.5]$ ,  $[5.8] - [8.0]$ ) and colour–magnitude ( $[3.6] - [8.0]$ ,  $[8.0]$ ) diagrams of these C-rich objects, with a large infrared emission, traces an obscuration sequence, according to the amount of carbonaceous dust in their surroundings. The overall population of C-rich AGB stars descends from  $1.5\text{--}2 M_{\odot}$  stars of metallicity  $Z = 4 \times 10^{-3}$ , formed between 700 Myr and 2 Gyr ago, and from lower metallicity objects, of mass below  $1.5 M_{\odot}$ , 2–5 Gyr old. We also identify obscured oxygen-rich stars ( $M \sim 4\text{--}6 M_{\odot}$ ) experiencing hot bottom burning. The differences between the AGB populations of the SMC and LMC are also commented.

**Key words:** stars: abundances – stars: AGB and post-AGB – ISM: abundances.

## 1 INTRODUCTION

Stars evolving through the asymptotic giant branch (AGB) phase are regarded as important dust manufacturers (Gehrz 1989). The winds of AGB stars are an extremely favourable environment to dust formation, owing to the high densities and the relatively low temperatures, which favour condensation of gas molecules into dust grains (Gail & Sedlmayr 1985, 1999). For these reasons, knowledge of dust production from AGB stars proves important for a number of astrophysical contexts: the interpretation of the spectral energy distribution (SED) of high-redshift quasars (Bertoldi et al. 2003; Wang et al. 2008, 2013); the study of dust evolution in galaxies of the Local Group (Dwek 1998; Calura, Pipino & Matteucci 2008; De Bressan et al. 2014; Schneider et al. 2014); the possible explanations of the presence of dust at early epochs (Valiante et al. 2009, 2011; Pipino et al. 2011). Furthermore, the debate concerning the relative contributions from different kinds of stars to the overall

dust budget is still alive: the early claim of a dominant contribution from supernovae (Maiolino et al. 2004) was challenged by following investigations, focused on the effects of the reverse shocks on dust destruction (Bianchi & Schneider 2007). The important contribution from AGB stars to dust production at high redshifts was outlined by Valiante et al. (2009).

Modelling dust formation around AGB stars have made significant progresses in the last few years. The pioneering investigations by the Heidelberg group (Ferrarotti & Gail 2001, 2002, 2006) were followed by works from other research teams (Ventura et al. 2012a,b, 2014b; Di Criscienzo et al. 2013; Nanni et al. 2013a,b, 2014). The results found by the various groups present considerable differences in the amount of dust produced by AGB stars and the kind of particles formed (Nanni et al. 2013b). This is due to the different input physics used, particularly for what concerns the most relevant factors affecting AGB evolution, i.e. convection and mass-loss (Ventura & D’Antona 2005a,b; Doherty et al. 2014).

Unfortunately, despite some admirable attempts (Canuto 1992, 1993), we are still far from an exhaustive description of the convective phenomenon, accounting for non-locality, based on a

\* E-mail: flaviadellaghi@gmail.com

self-consistent solution of the Navier–Stokes equations; this approach would be the only way to determine, based on first principles, the efficiency of the convective transport of energy and the mixing induced by convective eddies.

Therefore, the only possibility to achieve a more reliable description of the AGB phase, with a higher predictive power of the results obtained, is to fix the main properties of AGB stars via a detailed comparison with the observations. The Magellanic Clouds (MCs) are the ideal environments to this aim, owing to the relatively short distance (51 and 61 Kpc, for the Large Magellanic Cloud (LMC) and the Small Magellanic Cloud (SMC), respectively, Cioni et al. 2000; Keller & Wood 2006) and the low reddening ( $E_{B-V} = 0.15$  and 0.04 mag, for the LMC and the SMC, respectively, Wasterlund 1997). The study of MCs, AGB stars offers better observational constraints to the theoretical models than their Galactic counterparts (e.g. García-Hernández et al. 2006, 2007, 2009) because of the unknown distances (and larger reddening) in our own Galaxy. The *Spitzer Space Telescope* made available to the community data of millions of AGB stars in the MCs: ‘Surveying the Agents of a Galaxy Evolution Survey’ (SAGE-LMC, Meixner et al. 2006) and the Legacy programme entitled ‘Surveying the Agents of Galaxy Evolution in the tidally stripped, low metallicity Small Magellanic Cloud’ (SAGE-SMC, Gordon et al. 2011) have provided spatially and photometrically complete infrared surveys of the evolved star population in the MCs.

Dell’Agli et al. (2014b) and Dell’Agli et al. (2015, hereinafter D15), in a recent investigation, used dusty AGB models to study the AGB population of the LMC. The theoretical results were compared to *Spitzer* data from Riebel et al. (2012). D15 presented an interpretation of the observed sample of AGB stars, by characterizing the stars in terms of age, mass of the progenitors, chemical composition, dust in the circumstellar envelope. The comparison among the observed and expected distribution of AGB stars in the colour–colour and colour–magnitude diagrams obtained with the *Spitzer* infrared bands allowed the determination of the relative contributions from C-stars and oxygen-rich AGB stars. The most relevant result was the study of the most obscured sources, called ‘extreme’: the stars were identified as a majority of C-rich stars, in the final evolutionary AGB phases, and a smaller group of younger objects, undergoing Hot Bottom Burning (hereinafter HBB). The study of D15 provided an important feedback on the details of AGB modelling, particularly for what concerns the depth of the Third Dredge-Up (TDU). The possibility that the IR colours of massive AGB stars, associated with a measure of the C/O ratio, can be used to determine the efficiency of HBB, was investigated by Ventura et al. (2015).

In this paper, we extend to the SMC the analysis applied by D15 to the LMC. The goal of this investigation is to compare our interpretation of the SMC population of AGB stars with the classification of the sources observed, present in the literature. To this aim, similarly to D15, we attempt a characterization of the stars observed to infer their mass, formation epoch, surface chemistry and the dust in their surroundings. A particular attention is dedicated to the stars with the largest infrared emission, to derive their contribution to dust production in the SMC. For this reason, we base the comparison among models and observations on the four IRAC filters centred at 3.6, 4.5, 5.8, 8.0  $\mu\text{m}$ , covering the wavelength range where most of the infrared emission from obscured, dusty AGB stars occurs.

This investigation will be an important test for the theories regarding the evolution of AGB stars and the dust formation process in their winds. The analysis by D15 showed that the current generation of AGB models is able to satisfactorily reproduce the obscured AGB

population in the LMC. To assess the reliability of these models, it is crucial to understand whether the same description of convection and mass-loss used in D15, and the schematization of the dust formation process adopted in that work, allows the description of the AGB population in a galaxy with a different total mass, star formation history (SFH), age–metallicity relations, as the SMC is. Because the SFH of the LMC and SMC show important differences (Harris & Zaritsky 2004, 2009), this work offers the opportunity to test AGB models in a different range of mass and metallicity, with respect to those used by D15 (see also Schneider et al. 2014).

This work is to be considered a first, important step, towards the description of the AGB population in more distant environments, and to estimate their contribution to dust production. This study will help to be prepared in the future, to take advantage of the many, challenging opportunities, offered by the incoming observational facilities.

The paper is organized as follows: the data set of AGB stars in the SMC used for our analysis is described in Section 2; the numerical and physical input used to model the AGB phase and the dust formation process, and to produce the synthetic population of AGB stars are given in Section 3; Section 4 presents the main results concerning the evolution properties of AGB stars and of the dust in their surroundings; the interpretation of the observations is discussed in Section 5, while a comparison of our results with the classification by Boyer et al. (2011) is given in Section 6. Finally, Section 7 compares the AGB populations in the SMC and LMC and our conclusions are offered in Section 8.

## 2 AGB STARS IN THE SMC: OBSERVATIONS AND CLASSIFICATIONS

The SMC is a valuable environment to study evolved stars and their contribution to life cycle of dust in the Universe. This stems from the relative proximity ( $\sim 61$  kpc) and the low interstellar medium (ISM) metallicity. Several SMC infrared surveys have been conducted so far: *IRAS* (Schwering & Israel 1989; Miville-Deschenes & Lagache 2005), the *Infrared Space Observatory (ISO)* (Wilke et al. 2003), and *MSX* (Price et al. 2001). The growing interest towards this galaxy has stimulated more recent near-IR and mid-IR surveys of the SMC: the AKARI survey (Ita et al. 2010) of small selected regions within the SMC bar and the *Spitzer* Survey of the Small Magellanic Cloud (S3MC; Bolatto et al. 2007), which imaged the SMC bar.

The photometric data from the *Spitzer* Legacy programme ‘Surveying the Agents of Galaxy Evolution in the SMC’ (SAGE-SMC Gordon et al. 2011) provides a high-resolution, uniform, unbiased survey of the whole galaxy, including bar, wing and tail. Images were obtained in a 30 deg<sup>2</sup> field with *IRAC* (3.6, 4.5, 5.8, and 8  $\mu\text{m}$ ) and *MIPS* (24, 70, and 160  $\mu\text{m}$ ) at two epochs.

Boyer et al. (2011) used the SAGE-SMC survey to investigate the infrared properties of the evolved stars in the SMC. On the basis of the position in photometric planes, they classified AGB stars into four groups: oxygen-rich stars (O-AGB), anomalous oxygen-rich (aO-AGB), carbon stars (C-AGB) and ‘extreme’ stars (X-AGB). C-AGB and O-AGB stars were classified in the  $J - K_s$  versus  $K_s$  plane, following the cuts proposed by Cioni et al. (2006a) and rescaling for metallicity and distance, as in Cioni et al. (2006b) (see also section 3.1.1 in Boyer et al. 2011). To exclude contamination from RGB stars, the authors considered only objects brighter than the tip of the red giant branch (TRGB), with  $K < K_s^{\text{TRGB}} = 12.58$  mag (Cioni et al. 2000) and  $[3.6] < [3.6]_{\text{TRGB}} = 12.6$  mag. The X-AGB are the most obscured AGB stars in the sample. Owing to their efficiency in producing dust and their infrared emission, part of these

objects fall below the cuts used for the C-AGB and O-AGB (see section 3.1.2 in Boyer et al. 2011). Therefore, these sources were defined as those brighter than  $[3.6]_{\text{TRGB}}$  and with  $J - [3.6] > 3.1$ . If the near-IR radiation is completely obscured by dust, stars with  $[3.6] - [8.0] > 0.8$  are included in the X-AGB. Equations 1 and 2 in Boyer et al. (2011) describe the cuts used to minimize the contamination from young stellar objects (YSOs) and unresolved background galaxies.

In this paper, we compare the results from our theoretical models with the AGB sample presented in Boyer et al. (2011), following the selection described above. Our analysis is focused on the *IRAC* filters, therefore we exclude from the observational sample by Boyer et al. (2011) the objects which are missing the detection in at least one of these bands, which account for 1 per cent of the total. The resulting sample is constituted by  $\sim 5700$  stars.

We further tested our interpretation of the AGB population of the SMC against spectroscopically confirmed samples, observed in the last decades. Our analysis is mainly based on the recent work by Ruffe et al. (2015), who presented a detailed classification of 58 AGB stars of the SMC, using spectra taken with the *Spitzer Infrared Spectrograph*. We also compare our predictions with the stars analysed by Smith, Plez & Lambert (1995) and the results by García-Hernández et al. (2009), that presented high-resolution optical spectra (lithium and/or s-process element abundances) of a sample of unobscured and obscured AGB stars in the MCs. For these samples we did a cross-correlation with the observations by Boyer et al. (2011), to obtain the *Spitzer* magnitudes.

### 3 THE SIMULATION OF THE AGB POPULATION OF THE SMC

To compare the expected and observed distribution of stars in the various colour–colour and colour–magnitude diagrams obtained with the different *IRAC* filters, we followed a synthetic approach.

We assume the SFH of the SMC given by Harris & Zaritsky (2004). A plot of the variation with time of the star formation rate (SFR) is given in Fig. 1. Note that in the work by Harris & Zaritsky (2004) the total SFH is split into three stellar components, of metallicity  $Z = 10^{-3}$ ,  $Z = 4 \times 10^{-3}$  and  $Z = 8 \times 10^{-3}$ .

#### 3.1 Stellar evolution modelling

The evolutionary sequences of central stars were calculated by means of the *ATON* code for stellar evolution (Mazzitelli 1989). The numerical structure of the code is described in details in Ventura et al. (1998), whereas the latest updates are given in Ventura & D’Antona (2009).

As stated previously, we used three sets of models, with metallicity  $Z = 10^{-3}$ ,  $Z = 4 \times 10^{-3}$  and  $Z = 8 \times 10^{-3}$ . The initial helium was  $Y = 0.25$  for the most metal-poor population, and  $Y = 0.26$  for  $Z = 4 \times 10^{-3}$  and  $Z = 8 \times 10^{-3}$ . The relative percentages of the various chemical species are taken from Grevesse & Sauval (1998). We assumed an alpha-enhancement  $[\alpha/\text{Fe}] = +0.4$  for the  $Z = 10^{-3}$  case, and  $[\alpha/\text{Fe}] = +0.2$  for the higher metallicities.

All the evolutionary sequences were followed from the pre-main sequence, until the almost total consumption of the external envelope.

We recall here the main physical input used in the computations, most relevant for this work.

The convective instability was described according to the Full Spectrum of Turbulence (hereinafter FST) model, discussed in details in Canuto & Mazzitelli (1991). Convection modelling is the

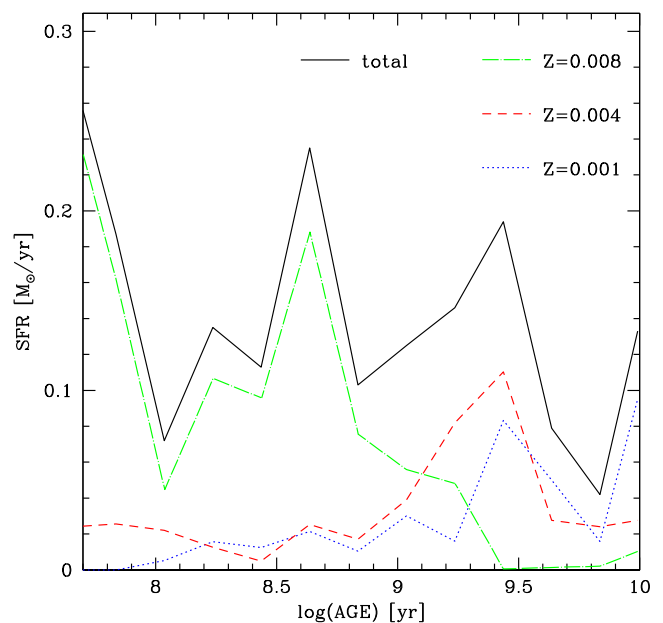


**Figure 1.** The SFH of the SMC as a function of stellar age (present time is  $t = 0$ ), according to Harris & Zaritsky (2004). The solid (black) line gives the total SFH, whereas the dotted (blue), dashed (red), dot-dashed (green) tracks give the contributions from stellar populations of metallicity, respectively,  $Z = 10^{-3}$ ,  $Z = 4 \times 10^{-3}$  and  $Z = 8 \times 10^{-3}$ .

most relevant factor in determining the time-scale of the AGB evolution and the modification of the surface chemistry. As shown by Ventura & D’Antona (2005a), use of the FST description makes massive AGB stars, with initial mass above  $\sim 3 M_{\odot}$ , to experience strong HBB. This has the double effect of shortening the evolutionary times and to modify the surface chemistry, according to the equilibria of proton-capture nucleosynthesis.

Mixing in convective regions is treated as a non-instantaneous process, coupled with nuclear burning. For each chemical species we solve a diffusion-like equation, following the schematization by Cloutmann & EoII (1976). This approach demands the computation of convective velocities, entering the diffusive coefficient. Within this framework, the overshoot phenomenon, i.e. the penetration of convective eddies in regions formally stable against convective motions, is described via the decay of velocities beyond the formal border, fixed via the Schwarzschild criterion. We use an exponential decay of velocities into radiatively stable regions, with an e-folding distance  $l = \zeta H_p$ , where the pressure scaleheight,  $H_p$ , is calculated at the formal border of convection. During the core hydrogen and helium burning phases, we used  $\zeta = 0.02$  to describe overshoot from the border of the convective core and the base of the stellar envelope; this is in agreement with the calibration of the width of the main sequences of open clusters, given in Ventura et al. (1998). During the thermal pulses phase, we used  $\zeta = 0.002$  to model extra-mixing from the bottom of the surface mantle and the borders of the convective shell which forms in conjunction with the ignition of each thermal pulse; the latter value is based on the calibration of the luminosity function (LF) of carbon stars in the LMC (Ventura et al. 2014b).

The description of mass-loss is also a crucial ingredient for the modelling of the AGB phase. The rate of mass loss determines the duration of the whole AGB evolution, the number of thermal pulses experienced and, consequently, the modification of the surface chemistry (Ventura & D’Antona 2005b; Doherty et al. 2014).

For oxygen-rich stars we used the description of mass-loss by Blöcker (1995), based on hydrodynamic simulations by Bowen (1988). For carbon stars, we used the formulae giving the mass-loss rate as a function of luminosity and effective temperature published by the Berlin group (Wachter et al. 2002, 2008). This treatment is based on pulsating hydrodynamical models, in which mass-loss is driven by radiation pressure on dust grains.

For what concerns the modelling of carbon stars, the computation of the low-temperature molecular opacities for carbon-rich mixtures has a great impact on the results. This is because when the C/O ratio becomes larger than unity, the formation of CN molecules favours a considerable increase in the molecular opacities of the external layers of the star; this, in turn, leads to an overall expansion of the whole outer region of the stars, and to an increase in the rate of mass-loss. Under these conditions, the star loses the external mantle very rapidly, thus limiting the number of thermal pulses experienced (Marigo 2002). The interested reader may find in Ventura & Marigo (2009, 2010) a detailed discussion on this argument, and the relative implications for the AGB evolution.

In the models used here, we calculated the molecular opacities in the stellar surface layers (temperatures below 10 000 K) by means of the *AESOPUS* tool (Marigo & Aringer 2009). The tables generated with the *AESOPUS* code are available in the range of temperatures  $3.2 \leq \log T \leq 4.5$ . The reference tables assume the same initial composition of the models used in this work. For each combination of metallicity and  $\alpha$ -enhancement, additional tables are generated, in which the reference mixture is altered by varying the abundances of C, N and O. This step is done by introducing the independent variables  $f_C, f_N, f_{CO}$ , that correspond to the enhancement (in comparison with the initial stellar chemistry) of carbon, nitrogen and of the C/O ratio, respectively.

### 3.2 The formation and growth of dust grains

The winds of AGB stars are a favourable environment for the formation and growth of dust grains. This stems from the low temperatures of their surface layers, which allow the formation of dust grains close to the stellar surface, at typical distances of  $\sim 1-10R_*$  ( $R_*$  is the stellar radius): in those regions the gas densities are sufficiently large to allow dust formation in great quantities (Gail & Sedlmayr 1985, 1999).

The model for the growth of dust grains in the circumstellar envelopes of AGB stars is described in details in the previous papers by our group (Ventura et al. 2012a, 2014b, 2012b; Di Criscienzo et al. 2013), where all the relevant equations, describing the thermodynamic structure of the wind and the rate of growth of the various dust species, are given.

The outflow is spherically symmetric, and it expands isotropically from the surface of the star, with an initial velocity  $v_0 = 1$  km/s. The formation of dust particles favours the acceleration of the wind, owing to the action of radiation pressure on the dust grains. The latter effect depends on the extinction coefficient, describing the interaction between the radiation from the star and the solid particles of a given species.

The kind of particles formed is determined by the surface C/O ratio. In the winds of oxygen-rich stars formation of silicates occurs, at a distance that, depending on the effective temperature, is in the range  $d \sim 5-10R_*$  from the stellar surface; also small quantities of solid iron are present. The most stable species is alumina dust ( $Al_2O_3$ ), which forms at a typical distance of  $\sim 1-3$  stellar radii from the stellar surface (Dell’Agli et al. 2014a). In carbon-rich environments we find a similar situation, with a stable and extremely

transparent dust species, silicon carbide (SiC), forming close to the surface of the star ( $d \sim 1-2R_*$ ), surrounded by a more external region ( $d \sim 5R_*$ ), where solid carbon grains form and grow.

The amount of a given dust species which can be formed depends on the surface mass fraction of the so called ‘key-element’, i.e. the least abundant chemical species, concurring in the condensation process.

A list of the various dust species used in this work, with the list of key species and the references for the optical constants adopted, are given in Table 1.

The description of the wind is interfaced with the AGB evolution modelling, because the results obtained depend on the main physical quantities of the central stars, namely effective temperature, mass loss rate, luminosity, surface gravity.

### 3.3 Synthetic spectra

The evolutionary models of AGB stars provide the variation of the main physical and chemical quantities of the star during the whole thermal pulses phase, allowing us to follow the behaviour of luminosity, effective temperature, rate of mass-loss, and of the surface chemical composition. The application of the dust formation model, described in Section 3.2, leads to the determination of the amount of dust formed in the wind, distributed among the different dust species, reported in Table 1. The knowledge of the density and grain size stratification of the wind allows the computation of the optical depth, which gives an indication of the degree of obscuration of the radiation emitted from the surface of the star.

All these ingredients are used to derive the SED of the star for some selected models along the evolutionary sequence. To this aim, we used the code *DUSTY* (Nenkova, Ivezić & Elitzur 1999).

The input radiation from the central star was obtained by interpolating in gravity and effective temperature among the appropriate tables of the same metallicity: we used the *NEXTGEN* atmospheres (Hauschildt et al. 1999) for oxygen-rich stars, whereas the *CO-MARCS* atmospheres (Aringer et al. 2009) were adopted for carbon stars; in the latter case we interpolated among the C/O values.

The effects of dust on the redistribution of the radiation from the star was calculated by accounting for the effects of two dusty layers. In the innermost regions, we consider the contribution from the most stable dust species, i.e. alumina dust for oxygen-rich AGB stars and SiC for carbon stars. The radiation emerging from this more internal zone is further reprocessed by a more external dusty layer, populated by grains of alumina dust and silicates in the case of stars with a surface C/O < 1; for carbon stars, this more external region is populated by solid particles of SiC and amorphous carbon.

Convolution of the emerging flux with the transmission curves of the different bands allows calculating the various magnitudes and colours.

## 4 THE EVOLUTION OF AGB STARS

This work is based on the models of AGB evolution and of the dust formation process in the wind, used in D15. Section 3 of D15 provides an exhaustive description of the evolution of AGB stars of different mass, in the range of metallicities of interest here, and of the change in their SED during the various AGB phases: this allows the description of the path traced by the evolutionary tracks in the colour–colour and colour–magnitude planes. An overview of the main results discussed in D15 is given in the following.

**Table 1.** The dust species considered in this work.

Dust species	Formula	Environment	Key species	Optical constants
Olivine	Mg <sub>2</sub> SiO <sub>4</sub>	O-rich	Si	Ossenkopf, Henning & Mathis (1992)
Pyroxene	MgSiO <sub>3</sub>	O-rich	Si	Ossenkopf et al. (1992)
Quartz	SiO <sub>2</sub>	O-rich	Si	Ossenkopf et al. (1992)
Corundum	Al <sub>2</sub> O <sub>3</sub>	O-rich	Al	Koike et al. (1995)
Iron	Fe	O-rich; C-rich	Fe	Ordal et al. (1988)
Carbon	C	C-rich	C	Hanner (1988)
Silicon carbide	SiC	C-rich	Si	Pegourie (1988)

#### 4.1 AGB stars: physical properties and the surface chemistry

The main evolution properties of the models used here are discussed in details in Ventura et al. (2013) for the metallicities  $Z = 10^{-3}$  and  $Z = 8 \times 10^{-3}$ , and in Ventura et al. (2014a) for  $Z = 4 \times 10^{-3}$ . The interested reader is referred to these two papers for a detailed description of the AGB phase. Here, we give a summary of the main evolutionary properties.

During the AGB phase the stars undergo a series of thermal pulses, when ignition of  $3\alpha$  reactions in a helium-rich buffer above the degenerate core occurs, and the CNO burning shell is temporarily extinguished. The external envelope is gradually lost by stellar wind. Eventually, nuclear reactions in the H-burning shell are extinguished, and the evolutionary tracks first moves to the blue region of the Hertzsprung–Russell diagram, before beginning the white dwarf cooling. This event marks the end of the AGB phase, thus determining its overall duration.

The luminosity of AGB stars increases with the initial mass,  $M_{\text{init}}$ , of the star: the higher is  $M_{\text{init}}$ , the higher is the mass of the degenerate CO core,<sup>1</sup> the brighter is the star (see left-hand panel of fig. 1 in Ventura et al. 2013). The luminosities of AGB stars cover a range of approximately one order of magnitude, from  $L \sim 10^4 L_{\odot}$  ( $M_{\text{init}} \sim 1 M_{\odot}$ ), to  $L \sim 10^5 L_{\odot}$ , for  $M_{\text{init}} \sim 7.5\text{--}8 M_{\odot}$ .

This reflects into a difference in the duration of the whole AGB phase, depending on the stellar mass (see table 1 in D15). Our computations indicate that the AGB phase of low-mass AGB stars lasts  $\sim 1$  Myr, whereas their counterparts of highest mass loose the external envelope within a few tens of kyr. We reiterate here that the evolution times are rather uncertain, as they depend on the input physics used to calculate the evolutionary sequences (Ventura & D’Antona 2005a; Doherty et al. 2014).

The surface chemical composition changes during the AGB life, according to the relative contributions of TDU and HBB. The former favours a gradual increase in the surface carbon that eventually can lead to the formation of a carbon star. HBB consists in the ignition of nuclear burning in the innermost regions of the convective envelope; the resulting change in the surface chemistry reflects the equilibria of proton-capture nucleosynthesis. HBB is activated when the temperature at the bottom of the convective envelope exceeds  $\sim 40$  MK. This demands a minimum core mass of  $\sim 0.8 M_{\odot}$ , which reflects into a constrain on the initial mass of the star:  $M_{\text{init}} > 3 M_{\odot}$  (see right-hand panel of fig. 1 in Ventura et al. 2013). The most prominent effect of HBB is the destruction of the surface carbon, via proton capture.

<sup>1</sup> Indeed, models with mass in the range  $6.5 M_{\odot} \leq M \leq 8 M_{\odot}$  develop a core made up of oxygen and neon, after an off-centre carbon ignition, and the following development of a convective flame, propagating inwards, until reaching the centre of the star.

This introduces a dichotomy in the evolution of the surface chemistry of AGB stars.

(i) Low-mass AGB stars,  $1 M_{\odot} < M_{\text{init}} < 3 M_{\odot}$ ,<sup>2</sup> evolve as carbon stars. The enrichment in carbon depends on the number of TDU episodes experienced, and is therefore higher for larger values of  $M_{\text{init}}$ : models with  $M_{\text{init}} \sim 2.5\text{--}3 M_{\odot}$  achieve the largest surface abundances of carbon. The ejecta of these stars will therefore be enriched in carbon and, at a lower extent, in oxygen.

(ii) High-mass AGB stars, with  $M_{\text{init}} > 3 M_{\odot}$ , experience HBB, thus remaining oxygen-rich. The temperatures of the regions close to the bottom of the convective envelope increase with  $M_{\text{init}}$  (see right-hand panel of fig. 1 in Ventura et al. 2013). However, the trend of the degree of the nucleosynthesis experienced with  $M_{\text{init}}$  is not straightforward, as it depends on the delicate interplay between the temperatures in the envelope and the rate of mass loss (Ventura, & D’Antona 2011). The gas expelled by massive AGB stars will be greatly enriched in nitrogen, and reduced in carbon and oxygen (see fig. 1 in Ventura et al. 2014a).

The modification of the surface chemistry is sensitive to the metallicity of the star. Models of smaller metallicity experience stronger HBB, thus the proton-capture nucleosynthesis occurs at higher temperatures, provoking a greater change in the mass fractions of the various elements involved. This not only reflects into the CNO elements, as shown in fig. 1 in Ventura et al. (2014a), but also into the production of sodium and aluminium (see figs 2 and 3 in Ventura et al. 2014a). Turning to the AGB stars of lower mass, the C-star stage is reached more easily in models of smaller metallicity, owing to the lower initial content of oxygen in the gas from which the star forms.

#### 4.2 Dust from AGB stars

As discussed in Section 3.2, the latest generation of AGB models involve also dust formation in the circumstellar envelope. The models published so far rely on the schematization by the Heidelberg group (Ferrarotti & Gail 2006), where the growth of dust grains takes place in an isotropically, expanding wind, moving outwards from the surface of the star. This schematization was used in the recent explorations by Nanni et al. (2013a,b, 2014) and in the previous works on this argument by our group (Ventura et al. 2012a,b; Di Criscienzo et al. 2013; Dell’Agli et al. 2014a).

The dependence of dust production on the initial mass and the metallicity of AGB stars was described in details in Ventura et al.

<sup>2</sup> The threshold mass separating stars evolving as carbon stars from more massive objects, experiencing HBB, changes with the metallicity. It is  $3 M_{\odot}$  for  $Z \geq 4 \times 10^{-3}$ , whereas it is  $\sim 2.5 M_{\odot}$  for lower metallicity stars (see e.g., Ventura et al. 2013)

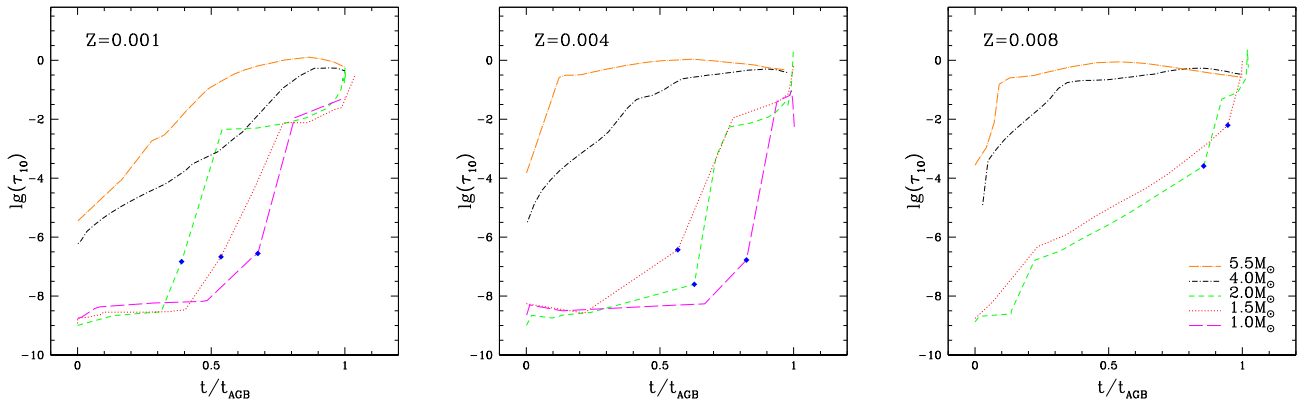


**Figure 2.** The variation during the AGB evolution of the optical depth,  $\tau_{10}$ , of AGB models of different initial mass and metallicity  $Z = 10^{-3}$  (left-hand panel),  $Z = 4 \times 10^{-3}$  (middle) and  $Z = 8 \times 10^{-3}$  (right-hand panel). Times on the abscissa are normalized to the total duration of the AGB phase. Blue squares along the tracks mark the beginning of the C-star phase. In the right-hand panel, we do not show  $1 M_{\odot}$  model at  $Z = 8 \times 10^{-3}$ , which does not become a C-star.

(2014b), where the uncertainties affecting the results are also discussed.

Based on the arguments of the previous section, SiC and solid carbon grains form in the winds of AGB stars of initial mass  $1 M_{\odot} < M_{\text{init}} < 3 M_{\odot}$ , whereas AGB stars of higher mass will be surrounded by silicates and alumina dust grains.

The amount of SiC formed in low-mass AGB stars scales with metallicity, as the corresponding key element, silicon, is proportional to  $Z$ . We find that the typical size of SiC grains formed is 0.05, 0.07, 0.08  $\mu\text{m}$ , for AGB stars of metallicity  $Z = 10^{-3}$ ,  $Z = 4 \times 10^{-3}$ ,  $Z = 8 \times 10^{-3}$  (see fig. 5 in Ventura et al. 2014b). The mass of silicon carbide produced is  $M_{\text{SiC}} \sim 10^{-5} - 4 \times 10^{-5} M_{\odot}$  for  $Z = 10^{-3}$ ,  $M_{\text{SiC}} \sim 3 \times 10^{-5} - 3 \times 10^{-4} M_{\odot}$  for  $Z = 4 \times 10^{-3}$ ,  $M_{\text{SiC}} \sim 10^{-4} - 10^{-3} M_{\odot}$  for  $Z = 8 \times 10^{-3}$  (fig. 4 in Ventura et al. 2014b).

In C-rich environments the dust species produced in greatest quantities is solid carbon, despite being less stable than SiC: the reason is the much larger availability of carbon compared to silicon in the atmosphere of carbon stars. The amount of carbon dust formed increases with the stellar mass, because stars of higher mass experience more TDU episodes, thus achieve a greater carbon enrichment at the surface. Stars of initial mass  $M_{\text{init}} \sim 2 - 2.5 M_{\odot}$  are therefore the most efficient producers of carbon dust, with grain sizes of the order of  $\sim 0.2 \mu\text{m}$  in the circumstellar envelope (see fig. 5 in Ventura et al. 2014b). This result is approximately independent of metallicity, because the carbon accumulated at the surface is synthesized in the He-burning shell, and is independent of  $Z$ . The overall mass of carbon dust produced by low-mass AGB stars ranges from  $M_d \sim 10^{-3} M_{\odot}$  for stars of initial mass  $M_{\text{init}} \sim 1 M_{\odot}$ , to  $M_d \sim 10^{-2} M_{\odot}$  for  $M_{\text{init}} \sim 2 - 2.5 M_{\odot}$  (see fig. 3 in Ventura et al. 2014b).

In oxygen-rich stars, the mass of dust formed depends on the metallicity, because the key elements of the dust species formed, alumina dust and silicates, are aluminium and silicon, both dependent on  $Z$ . The size of the alumina grains formed are in the range 0.03–0.07  $\mu\text{m}$ , according to  $M_{\text{init}}$  and  $Z$ . The mass of alumina dust produced is below  $\sim 10^{-4} M_{\odot}$  for  $Z = 10^{-3}$ , whereas it is  $10^{-5} M_{\odot} < M_{\text{Al}_2\text{O}_3} < 10^{-3} M_{\odot}$  for the higher metallicities (see right-hand panel of fig. 9 in Ventura et al. 2014b). Most of the dust produced by oxygen-rich AGB stars is under the form of silicates, because the silicon content largely exceeds aluminium in the surface layers. The size of the dust grains formed increases with mass

and metallicity. The silicates with the largest size ( $\sim 0.15 \mu\text{m}$ ) form in the winds of massive AGB stars of metallicity  $Z = 8 \times 10^{-3}$  (fig. 8 in Ventura et al. 2014b). The overall mass of silicates produced is  $10^{-4} M_{\odot} - 10^{-3} M_{\odot}$  for  $Z = 10^{-3}$ , and in the range  $10^{-3} M_{\odot} - 10^{-2} M_{\odot}$  for  $Z = 4, 8 \times 10^{-3}$ .

### 4.3 The infrared spectra of AGB stars

Understanding the dust formation process in the wind of AGB stars is crucial to interpret the spectra of these stars, because the radiation emitted from the central star is reprocessed by dust particles in the infrared. The shape of the SED is determined by the dust species in the circumstellar envelope and by the optical depth, indicating the degree of obscuration of the star. Here we use  $\tau_{10}$ , the optical depth at the wavelength of 10  $\mu\text{m}$ .

Fig. 2 shows the evolution of  $\tau_{10}$  for the models used in this work; each panel corresponds to a single metallicity. For clarity reasons, we show only some of the masses involved in this analysis. To show all the tracks in the same plot, we use as abscissa the evolution time, normalized to the overall duration of the AGB phase.

Low-mass stars evolve initially as oxygen-rich; the optical depth is extremely small during this phase, because of the small amount of silicate dust in the envelope. After the carbon star stage is reached,  $\tau_{10}$  increases because more and more carbon is accumulated at the surface of the star, owing to the effects of TDU. In agreement with the discussion in Section 4.2, the highest  $\tau_{10}$  are reached by AGB stars of initial mass  $\sim 2 - 2.5 M_{\odot}$ , in the final evolutionary phases. The largest values of the optical depth,  $\tau_{10} \sim 3$ , are reached by the  $Z = 8 \times 10^{-3}$  models; low-mass AGB stars of  $Z = 10^{-3}$  evolve at optical depths below unity, whereas the  $Z = 4 \times 10^{-3}$  models show an intermediate behaviour. This can be explained as follows: higher- $Z$  models evolve at lower effective temperatures, which favours dust formation, because the region where gas molecules condense into dust is closer to the surface of the star, in a region of higher density.

The stars with initial mass above  $3 M_{\odot}$  experience HBB and behave differently. While in their counterparts of lower mass the optical depth depends strongly on the amount of carbon in the convective envelope, in massive AGB stars the dust formation process is mainly determined by the strength of HBB (Ventura et al. 2012a). The phase with the highest infrared emission occurs during the phase of strongest HBB, when both luminosity and mass loss rate reach their maximum values. The luminosity in these stars peaks

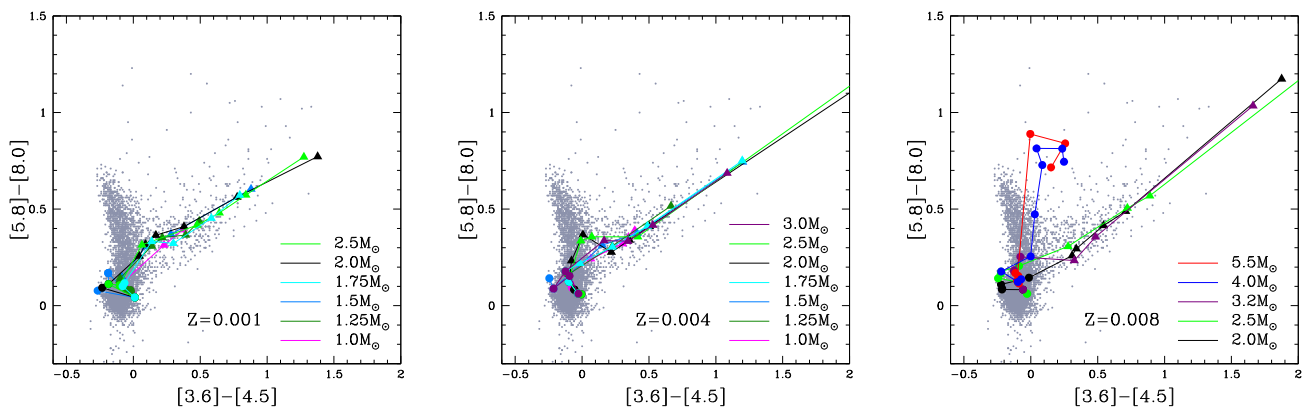


**Figure 3.** Evolutionary tracks in the colour–colour ( $[3.6] - [4.5]$ ,  $[5.8] - [8.0]$ ) plane of AGB stars of different initial mass and metallicity  $Z = 10^{-3}$  (left-hand panel),  $Z = 4 \times 10^{-3}$  (middle) and  $Z = 8 \times 10^{-3}$  (right-hand panel). The grey points represent data of AGB stars in the SMC from Boyer et al. (2011). Full circles indicate phases during which the stars are oxygen-rich, whereas full triangles correspond to carbon-rich objects.

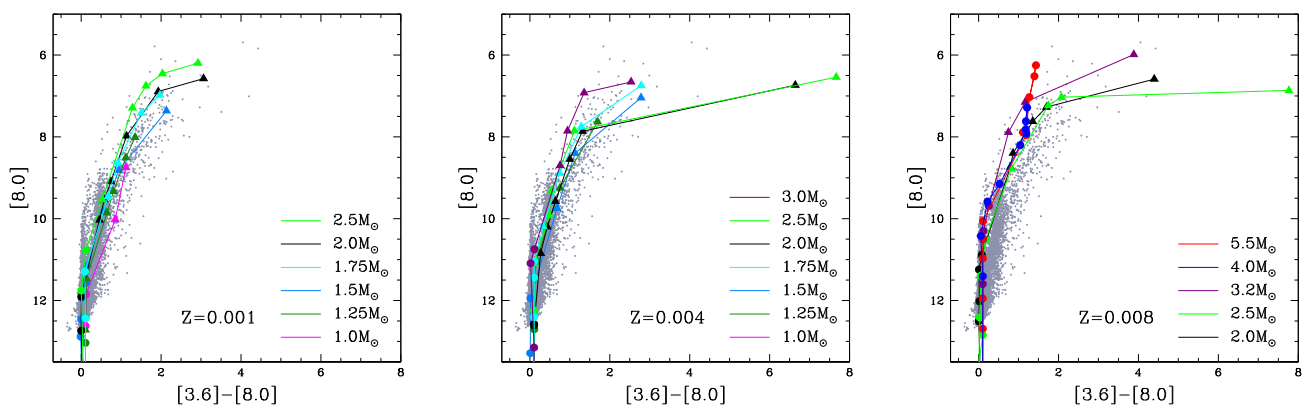


**Figure 4.** Evolutionary tracks in the colour–magnitude ( $[3.6] - [8.0]$ ,  $[8.0]$ ) plane of AGB stars of different initial mass and metallicity. The meaning of the symbols is the same as in Fig. 3.

in an intermediate evolutionary stage (see fig. 6 in Ventura et al. 2014b), when  $\tau_{10}$  is the highest shown. The tracks of the  $4 M_{\odot}$  and  $5.5 M_{\odot}$  models in the three panels of Fig. 2 reach the maximum  $\tau_{10}$  during the largest luminosity phase. Inspection of Fig. 2 confirms that oxygen-rich models of higher mass have a stronger infrared emission, because the strength of HBB increases with the initial mass of the star; this holds independently of the metallicity.

The highest degree of obscuration reached in these models,  $\tau_{10} \sim 1$ , is smaller than in their counterparts of smaller mass  $\tau_{10} \sim 3$ ; this is due to the larger content of carbon in low-mass AGB stars compared to the silicon in the external regions of more massive AGB stars; an additional motivation is that the extinction coefficient of solid carbon dust is higher than the corresponding coefficients of silicates.

#### 4.4 The infrared colours of AGB stars

Figs 3 and 4 show the evolutionary tracks of AGB models of various initial mass in the colour–colour ( $[3.6] - [4.5]$ ,  $[5.8] - [8.0]$ ) diagram (hereinafter CCD) and in the colour–magnitude ( $[3.6] - [8.0]$ ,  $[8.0]$ ) plane (CMD). For clarity reasons, we show some stellar models which, according to the SFH and the age–metallicity relationship of the SMC (see Fig. 1), will dominate the predicted synthetic population (see Fig. 5). In the same figures we show the observations from Boyer et al. (2011).

As shown in Fig. 2, stars with mass  $1 M_{\odot} < M_{\text{init}} < 3 M_{\odot}$  evolve at larger and larger optical depths as their envelope becomes more enriched in carbon. The tracks evolve to redder infrared colours, owing to the presence of carbonaceous dust particles in the surroundings of the star. In the CCD the models follow an evolutionary line of constant slope. Only models of mass  $M \geq 2 M_{\odot}$  evolve at  $[3.6] - [4.5] > 1.5$ , because they accumulate more carbon in the external regions, due to the higher number of thermal pulses experienced. The models of low metallicity do not reach such red colours; this is an effect of their higher effective temperature, as discussed in Section 4.3. In the CMD, the main effect of the gradual carbon enrichment in the external regions of the stars is the rightwards excursion of the tracks, towards redder  $[3.6] - [8.0]$  colours. In this plane the threshold colour separating the  $Z = 10^{-3}$  models from their more metal rich counterparts is  $[3.6] - [8.0] \sim 3$ .

The stars with mass  $M_{\text{init}} > 3 M_{\odot}$  experience HBB and produce mainly silicates, with traces of alumina dust. During the maximum luminosity phase the stars reach their reddest IR colours. The infrared emission during these phases is sensitive to mass and metallicity, according to the discussion in the previous section (see Fig. 2). In the CCD the evolutionary tracks (see right-hand panel of Fig. 3) evolve to the region at  $[3.6] - [4.5] \sim 0.2$ ,  $[5.8] - [8.0] \sim 0.8$ . The tracks of these obscured AGB stars bifurcate from their counterparts of lower mass, owing to the presence of the silicates feature at  $9.7 \mu\text{m}$ , affecting the  $8.0 \mu\text{m}$  flux. A bifurcation among the C-rich

and the oxygen-rich tracks is also found in the CMD (see right-hand panel of Fig. 4), the latter evolving along a more vertical sequence.

## 5 AGB STARS IN THE SMC: UNDERSTANDING THE IR COLOURS

To interpret the *Spitzer* observations of AGB stars in the SMC, we produced synthetic diagrams in the CCD and CMD planes, with the same methods described in D15. For each epoch, we extracted a number of stars, proportional to the SFR by Harris & Zaritsky (2004), shown in Fig. 1. The mass distribution follows a standard Salpeter IMF with index  $x = -1$ , whereas the number of extractions for each mass scales with the overall duration of the AGB phase.

The mass and metallicity distribution of the stars extracted is shown in Fig. 5. In the mass domain of the stars experiencing HBB,  $M_{\text{init}} > 3 M_{\odot}$ , we note two peaks, at  $M \sim 4, 5.5 M_{\odot}$ ; the first corresponds to the peak in the SFH which occurred 150 Myr ago (see Fig. 1), whereas the maximum at  $M \sim 5.5 M_{\odot}$  concerns younger epochs,  $\sim 90$  Myr ago. These stars belong to the more metal-rich population, with metallicity  $Z = 8 \times 10^{-3}$ , which provided the greatest contribution during epochs younger than  $\sim 1$  Gyr. In the low-mass domain the dominant AGB population is given by  $Z = 4 \times 10^{-3}$  stars, with also a significant contribution from the low-metallicity component. The peak in the mass distribution around  $M = 1.5 M_{\odot}$  correspond to the peak in the SFH which occurred  $\sim 2.5$  Gyr ago (see Fig. 1).

The comparison among the observations of SMC AGB stars and the results from our synthetic modelling are shown in Figs 6 and 7. In the two figures we compare the observed (left-hand panels) and expected (right-hand panels) distribution of AGB stars in the CCD (Fig. 6) and CMD (Fig. 7) planes. The samples of spectroscopically confirmed AGB stars, described in Section 2, are also shown in the same figures. Figs 8 and 9 also show the comparison among the observation and theoretical predictions in the CCD and in CMD planes; in this case, however, the two panels show the distribution of carbon-rich stars (right-hand) and oxygen-rich stars (left-hand), divided among the various metallicity components.

### 5.1 Unobscured stars

The region of the CCD centred at  $[3.6] - [4.5] \sim -0.1$ ,  $[5.8] - [8.0] \sim +0.1$  is populated by AGB stars with an extremely small degree of obscuration, whose spectrum is not expected to show significant dust features. The red border of this region, (hereinafter region I), is represented by the diagonal line in Fig. 6, indicating stars with  $\tau_{10} \sim 0.001$ ; this choice is such that almost the totality of the oxygen-rich objects evolve bluewards of this line in the CCD (see Fig. 8). As shown in Fig. 3, the only exception here is represented by stars of initial mass above  $\sim 3 M_{\odot}$ , whose tracks cross the aforementioned line when HBB begins.

According to our interpretation, the majority ( $\sim 67$  per cent) of AGB stars in region I are low-mass, oxygen-rich stars, in the first part of the AGB phase, before the C-star stage is reached. They are distributed among  $Z = 4 \times 10^{-3}$  stars of mass  $1-2 M_{\odot}$  ( $\sim 27$  per cent),  $Z = 8 \times 10^{-3}$  AGB stars of mass  $2-3 M_{\odot}$  ( $\sim 23$  per cent),  $Z = 10^{-3}$  objects, of mass below  $2 M_{\odot}$  ( $\sim 17$  per cent).

A low fraction ( $\sim 4$  per cent) of stars in region I of the CCD is composed of  $Z = 8 \times 10^{-3}$  AGB stars of higher mass, in the phases previous to ignition of HBB; as discussed previously, and shown in Fig. 5, the mass distribution of these stars peaks at  $M \sim 4 M_{\odot}$  and  $M \sim 5.5 M_{\odot}$ . Scarcely obscured objects, classified as oxygen-rich stars in the sample by Ruffle et al. (2015) and Smith et al. (1995),

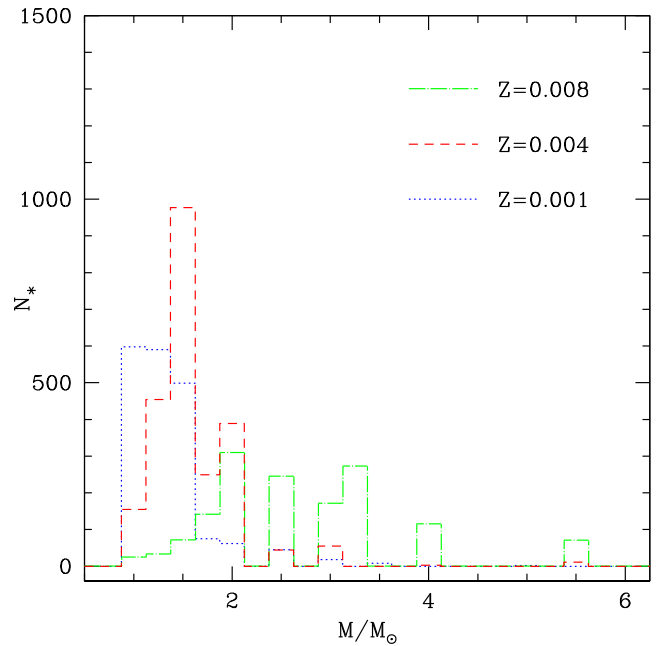


**Figure 5.** The mass distribution of the AGB population of the SMC, according to our synthetic modelling. The various masses are separated among the three different metallicities used in this analysis:  $Z = 10^{-3}$  (dotted, blue histogram),  $Z = 4 \times 10^{-3}$  (dashed, red),  $Z = 8 \times 10^{-3}$  (dot-dashed, green).

occupy this region of the CCD. The oxygen-rich stars presented by Smith et al. (1995) are divided among AGB stars with or without lithium. Unfortunately, the detection of lithium is of little help in this analysis, owing to the peculiar behaviour of this fragile element during the AGB evolution. Lithium is heavily destroyed by proton capture as soon as the AGB phase begins and is produced in great quantities when the temperature at the bottom of the surface convective region reaches  $\sim 40$  MK (Cameron & Fowler 1971). The lithium-rich phase lasts until some  ${}^3\text{He}$  is available in the envelope (Sackmann & Boothroyd 1992), thus it is limited to the initial part of the HBB phase (Mazzitelli, D’Antona & Ventura 1999). Based on these arguments, it is not surprising that some of the stars in the Smith et al. (1995) sample present evidence of lithium in their spectra; for similar reasons we understand that some of the oxygen-rich stars studied by Smith et al. (1995) with a large infrared emission (see Section 5.3 below) show no signature of lithium in their spectra.

As shown in the right-hand panel of Fig. 8, according to our modelling,  $\sim 29$  per cent of the sources populating region I are carbon stars, either at the very beginning of the C-star evolution, or in the evolutionary phases immediately following the ignition of each thermal pulse; these objects have a mixed metallicity: half of them are  $Z = 4 \times 10^{-3}$  AGB stars of mass  $M < 2 M_{\odot}$ , the remaining have metallicity  $Z = 10^{-3}$  and mass below  $M < 1.5 M_{\odot}$ . A word of caution is needed here. The comparison among the observations and our synthetic model shows the presence of a group of stars, in the region at  $[3.6] - [4.5] \sim -0.2$ ,  $[5.8] - [8.0] \sim +0.7$ , not reproduced by the models. We identify these stars as carbon-rich objects, not heavily obscured. The synthetic spectrum of these AGB stars is determined by the SED from the central object, substantially unchanged by the optically thin envelope. The blue  $[3.6] - [4.5]$  colours of these stars are not reproduced by the GRAMS atmosphere models used to produce the synthetic SED. This same problem was already addressed by D15, and is discussed in details by Srinivasan, Sargent &

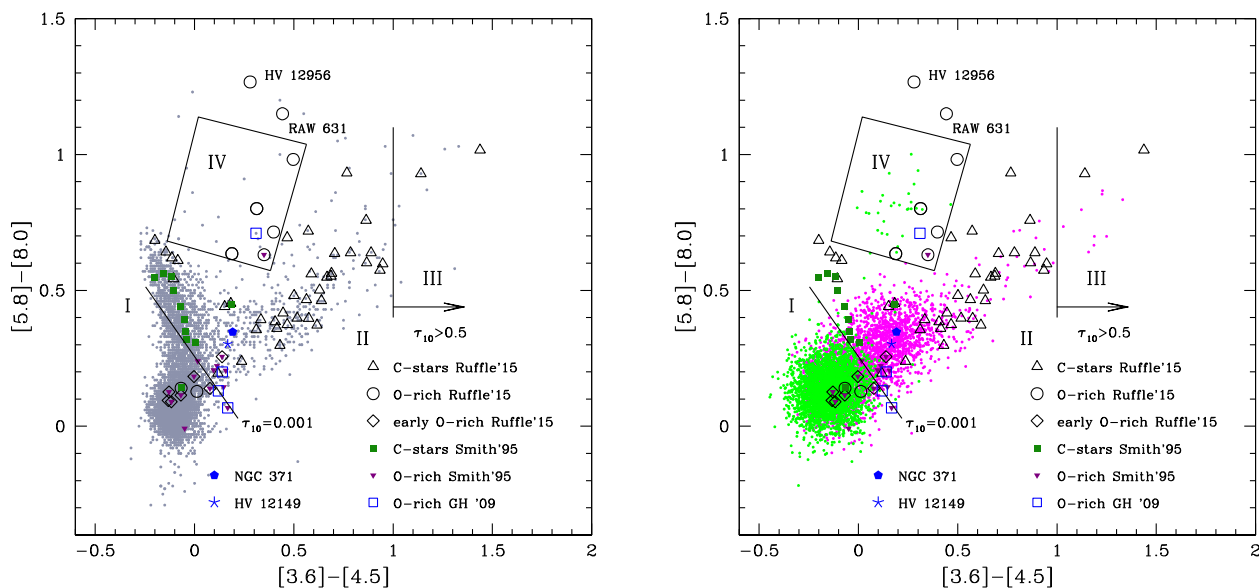


**Figure 6.** Left: the distribution of the AGB sample of the SMC by Boyer et al. (2011) in the colour–colour ( $[3.6] - [4.5]$ ,  $[5.8] - [8.0]$ ) plane. We show several spectroscopically confirmed samples: Ruffle et al. (2015), separated into carbon stars (black open triangles), oxygen-rich objects (black open circle) and early oxygen-rich objects (black open diamond), carbon stars (green full square) and oxygen-rich objects (violet full reversed triangle) by Smith et al. (1995) and oxygen-rich stars (blue open square) from García-Hernández et al. (2009). NGC 371 (Blue full diamond) and HV 12149 (blue star) are discussed in Section 5.3. Right: the results from our synthetic modelling in the same plane shown in the left-hand panel. Stars expected to be oxygen-rich are shown in green, whereas carbon stars are indicated in magenta. The spectroscopically confirmed samples by Ruffle et al. (2015), Smith et al. (1995) and García-Hernández et al. (2009) are also shown. The open square and the full triangle within region IV indicate, respectively, stars HV 1375 and IRAS 00483-7347, discussed in Section 5.3. The lines in the figure delimit regions I, II, III, IV, populated, respectively, by scarcely obscured AGB stars, carbon stars, extremely obscured carbon stars and stars experiencing HBB.

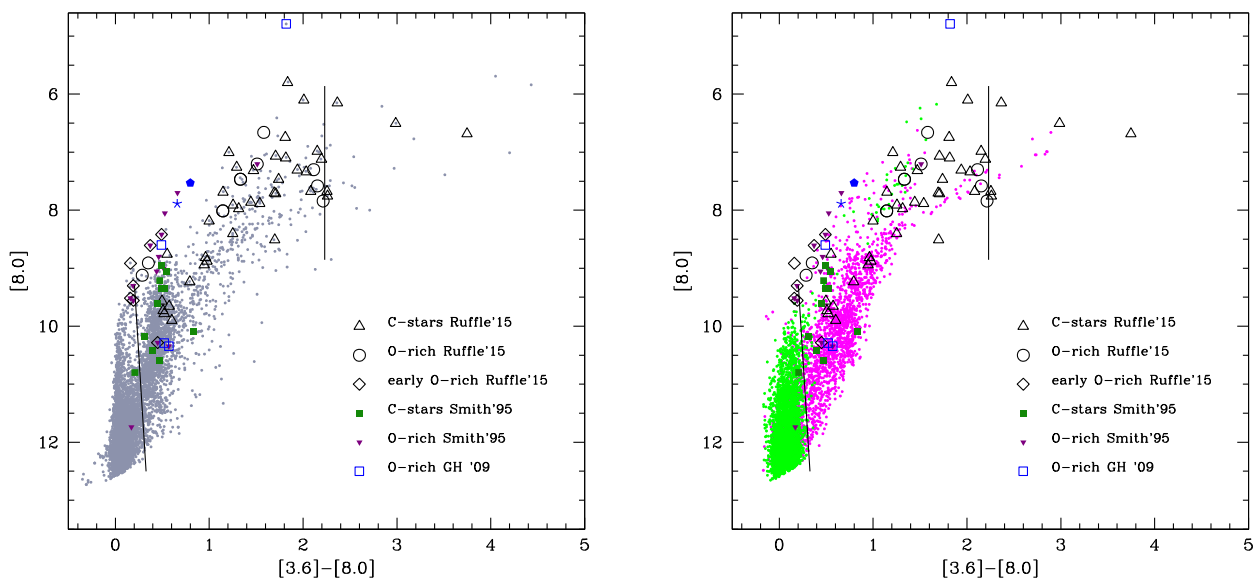


**Figure 7.** The same as Fig. 6, but referred to the colour–magnitude ( $[3.6] - [8.0]$ ,  $[8.0]$ ) plane. The line on the lower-left side of the diagram separates scarcely obscured objects (left-hand) from C-stars (right-hand), whereas the line at  $[3.6] - [8.0] \sim 2.2$  corresponds to the line on the right side of the CCD shown in Fig. 6. The spectroscopically confirmed samples by Ruffle et al. (2015), García-Hernández et al. (2009) and Smith et al. (1995) are shown, with the same symbols as in Fig. 6.

Meixner (2011, section 4.2.5). CO and  $C_3$  absorption bands could be a possible explanation of this discrepancy. We therefore suggest that part of the unobscured C-stars, which in our modelling evolve into region I of the CCD, would indeed populate the region in the higher portion of the CCD, currently uncovered by the models. C-stars in the Smith et al. (1995) sample populate this region of the colour–colour plane.

In the CMD, the group of scarcely obscured AGB stars populate the lower-left region. The  $[8.0] > 12$  mag zone (see left-hand panel of Fig. 9) is composed of stars of various surface chemistry. The sequences of C-stars and oxygen-rich AGB stars begin to bifurcate for  $[3.6] - [8.0] \sim 0.3$  and  $[8.0] < 12$  mag (see left-hand panel of Fig. 4): oxygen-rich stars trace a more vertical sequence, with  $[3.6] - [8.0]$  colours bluer than  $\sim 0.3$ , whereas carbon stars populate

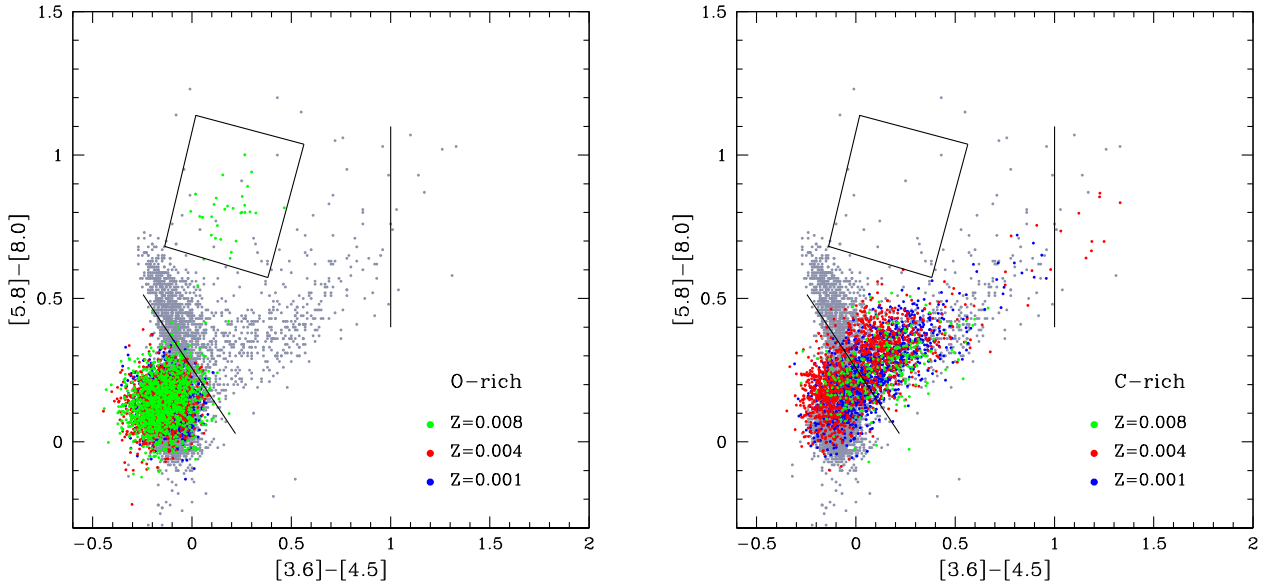


**Figure 8.** Left: the expected distribution of oxygen-rich stars from our synthetic modelling in the colour–colour ( $[3.6] - [4.5]$ ,  $[5.8] - [8.0]$ ) plane. We show the three metallicity components in different colours:  $Z = 8 \times 10^{-3}$  in green,  $Z = 4 \times 10^{-3}$  in red and  $Z = 10^{-3}$  in blue. The observed AGB sample from Boyer et al. (2011) is also shown in grey. Right: the expected distribution of carbon stars from our synthetic modelling in the colour–colour, with the same colour coding as in the left-hand panel.

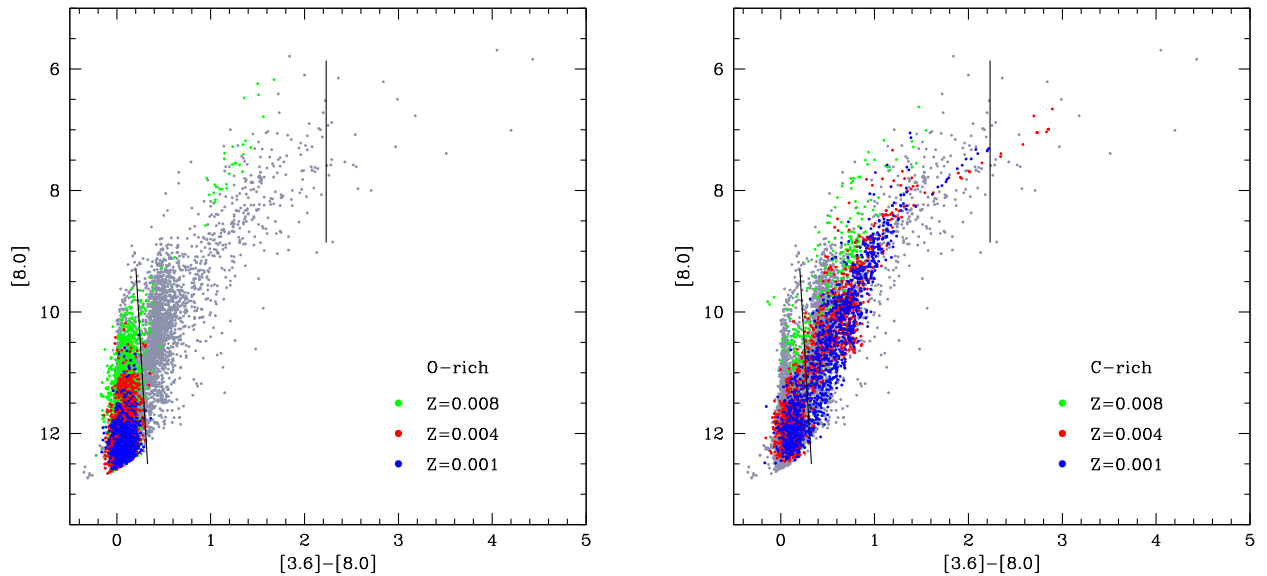


**Figure 9.** The same as Fig. 8, but referred to the colour–magnitude ( $[3.6] - [8.0]$ ,  $[8.0]$ ) plane.

the region  $[3.6] - [8.0] > 0.3$ . This effect, discussed in D15, originates from the silicate feature at  $\sim 9.7 \mu\text{m}$ , present in the spectra of dusty, oxygen-rich AGB stars: for a given  $[3.6] - [8.0]$  colour, the latter stars are brighter in the  $8.0 \mu\text{m}$  band, compared to their carbon-rich counterparts.

For what concerns oxygen-rich objects, the analysis of the distribution of the stars in the CMD, compared to the CCD, offers a better opportunity to disentangle stars of different metallicity; this is clearly shown in the left-hand panel of Fig. 9. While for magnitudes  $[8.0] > 11.5$  most of the stars belong to the population of lower metallicity, in the  $11 \text{ mag} < [8.0] < 11.5 \text{ mag}$  region we mainly find  $Z = 4 \times 10^{-3}$  objects, while for magnitudes  $[8.0] < 11$  we practically have only stars of metallicity  $Z = 8 \times 10^{-3}$ . This

is because the surface regions of higher metallicity models contain more silicon and aluminum, which favour the formation of larger amounts of silicates and alumina dust, and a higher degree of obscuration of the radiation from the central stars, hence a higher flux in the  $8.0 \mu\text{m}$  band. An additional motivation for this behaviour is that low-mass, higher metallicity AGB stars evolve longer as oxygen-rich objects, compared to their counterparts of lower  $Z$  (see Fig. 2); while the evolutionary tracks of the  $Z = 8 \times 10^{-3}$  (and, to a lower extent, of the  $Z = 4 \times 10^{-3}$ ) models follow the almost vertical sequence traced by oxygen-rich stars for the majority of the AGB life, the corresponding tracks of the  $Z = 10^{-3}$  models turn earlier (at higher  $[8.0]$  magnitudes) towards redder  $[3.6] - [8.0]$  colours.

## 5.2 Carbon stars

In the CCD, carbon stars populate a diagonal strip of constant slope, from the edge of region I towards red infrared colours. This is shown in Fig. 3, where the evolutionary tracks of low-mass AGB stars overlap with the observations by Boyer et al. (2011).

Similarly to D15, we interpret the AGB stars in region II of the CCD as an obscuration sequence of carbon stars: the objects with the largest infrared emission are those with the higher surface carbon content, which experienced a higher number of TDU episodes. The optical depth increases towards the red side of the sequence, owing to the large quantities of dust (mainly solid carbon grains) in the surroundings of these stars.

As stated previously, the blue border of region II was chosen in such a way that this region is almost exclusively populated by carbon stars; however, a small fraction of C-rich objects is also expected to populate region I in the CCD (see right-hand panel of Fig. 8).

The results shown in Fig. 6 indicate a satisfactory agreement among the observed and expected distribution of AGB stars in this region of the CCD; the colours of the theoretical models nicely fit the position of the carbon AGB stars sample by Ruffle et al. (2015).

Our analysis indicates that the carbon star sample in the SMC is composed of objects of metallicity  $Z = 4 \times 10^{-3}$  of mass  $1.5 M_{\odot} \leq M \leq 2 M_{\odot}$ , formed between 700 Myr and 1.5 Gyr ago and, in equal part, by low-mass ( $M < 1.5 M_{\odot}$ ) stars belonging to the  $Z = 10^{-3}$  stellar component, 1.5–5 Gyr old. Only 8 per cent of the carbon stars are objects of metallicity  $Z = 8 \times 10^{-3}$  of mass  $1.5 M_{\odot} < M < 3.5 M_{\odot}$ , formed between 300 Myr and 1.7 Gyr.

The stars with the largest infrared emission, with  $[3.6] - [4.5] > 1$ , populating region III in the CCD, descend from stars of metallicity  $Z = 4 \times 10^{-3}$  (see right-hand panel of Fig. 8) and initial mass  $M \sim 1.5 M_{\odot}$ ; according to our interpretation, these highly obscured objects formed  $\sim 1.5$  Gyr ago. The dust in their circumstellar envelope is mainly composed of solid carbon particles with size  $\sim 0.2 \mu\text{m}$ ; the optical depth of these stars is  $\tau_{10} > 0.5$ . Fig. 6 shows that the number of stars in this region of the CCD decreases as the colours become redder. This is partly because only the  $Z = 4 \times 10^{-3}$  stars reach the zone populated by the most obscured AGB stars; an additional reason is that the stars with the largest infrared emission lose more rapidly their external envelope, which makes the remaining evolutionary phases shorter (see fig. 3 in D15). The two carbon stars in the Ruffle et al. (2015) sample with the largest infrared emission belong to this group.

In the CMD plane, obscured carbon stars populate the region extending from  $[3.6] - [8.0] \sim 0.3$  to  $[3.6] - [8.0] \sim 4$ . The group of stars in the region included between the two lines in the CMD (see Fig. 7) is interpreted as composed mainly of carbon stars, with a small contribution from obscured, oxygen-rich AGB stars (see next section). The vertical line at  $[3.6] - [8.0] \sim 2.2$  delimits the region where the most obscured C-stars, populating region III in the CCD, evolve.

The position of the C-rich stars in the Ruffle et al. (2015) sample is nicely reproduced also in this plane.

## 5.3 AGB stars experiencing HBB

In the observed CCD of the SMC, (see Fig. 6), we see a few stars within region IV, with colours  $[3.6] - [4.5] \sim 0.1\text{--}0.3$ ,  $[5.8] - [8.0] \sim 0.5\text{--}1$ . According to our interpretation, based on the evolutionary tracks shown in the right-hand panel of Fig. 3, these

are the descendants of stars formed 100–400 Myr ago, with initial mass peaking at  $4 M_{\odot}$  and  $5.5 M_{\odot}$ , currently experiencing HBB. This group correspond to the AGB stars defined as ‘HBBS’ in D15 and it is composed only by stars with metallicity  $Z = 8 \times 10^{-3}$ , as shown in the left-hand panel of Fig. 8. The number of stars expected within region IV is a factor 2 greater than observed. If confirmed, this discrepancy would suggest that a significant production of dust in  $M \geq 4 M_{\odot}$  stars is limited to the phases close to the peak of HBB, with the highest rate of mass loss. This would demand a partial revision of the description of the massive AGB winds, which currently predicts considerable silicates formation since the early AGB phases (see fig. 5 in D15). Alternatively, we would consider possible effects of assuming the upper/lower limits of the SFH given by Harris & Zaritsky (2009). The relative contribution of stars formed in different epochs assuming the standard and lower limit are almost undistinguishable, while in the upper limit case a significantly higher number of massive AGB stars, formed 50–100 Myr ago, would be expected. This would further exacerbate the discrepancy among the observed and expected number of AGB stars in region IV of the CCD, pointing in favour of the standard or the lower limit. This cannot be a definitive conclusion though, as the low numbers involved (10 stars observed versus 20 expected) would require a deeper analysis of the statistical completeness of the sources detected in region IV. We leave this problem open.

In the CMD plane, the brightest oxygen-rich stars populate the region with  $6 \text{ mag} < [8.0] < 8 \text{ mag}$  and colours  $1 < [3.6] - [8.0] < 2$ ; their position partially overlaps with the AGB stars belonging to the sequence of C-rich objects. The colours and magnitudes of these objects are in nice agreement with the position of the most obscured, O-rich stars in the samples of spectroscopically confirmed stars in the CCD and CMD by Ruffle et al. (2015), García-Hernández et al. (2009) and Smith et al. (1995). It is very interesting that the most obscured (and extreme) O-rich SMC AGB stars, HV 1375 and IRAS 00483-7347 (spectroscopically confirmed by Smith et al. 1995 and García-Hernández et al. 2009, respectively), are inside region IV in the CCD. This seems to support our models: i) HV 1375 is a high-luminosity, Li-rich (HBB) AGB star, which is rich in s-process elements, like Zr and Nd, but Rb poor (Plez, Smith & Lambert 1993). The position in the CCD and CMD diagrams (Figs 6 & 7) is consistent with our predictions for a 4–5.5 solar mass AGB experiencing HBB, something consistent with the lack of Rb in this star (see García-Hernández et al. 2006, 2009); ii) IRAS 00483-7347 is the most massive HBB AGB star known to date in the SMC (as indicated by its extremely large Rb enhancement García-Hernández et al. 2009). Its position in the CMD, particularly the brightness in the  $8.0 \mu\text{m}$  band ( $[8.0] \sim 4.7 \text{ mag}$ ), indicates that this source is an AGB star of mass  $\sim 6\text{--}7 M_{\odot}$ .

We note in Fig. 6 the presence of two stars in the Ruffle et al. (2015) sample, RAW 631 and HV 12956, out of the region IV, in a zone of the CCD not covered by the evolutionary tracks (see Fig. 3). Both stars are heavily embedded and are sufficiently red ( $[8.0] - [24] > 2.39 \text{ mag}$ ) to be classified as far-IR objects, although they are not background galaxies, YSOs or PNe (see section 3.1.6 in Boyer et al. 2011, and section 5.1.3 in Ruffle et al. 2015). Their spectra also show evidence of crystalline silicates. RAW 631 present a dual chemistry, with absorption features from  $\text{C}_2\text{H}_2$  and HCN and strong features from crystalline silicates, reason why it was classified as oxygen-rich by Ruffle et al. (2015). These two objects present several peculiarities which renders difficult the modelling of their colours with the method we used for the other AGB stars.

Stars NGC 371, in the samples by Smith et al. (1995), and HV 12149, from Smith et al. (1995) and Ruffle et al. (2015), populating

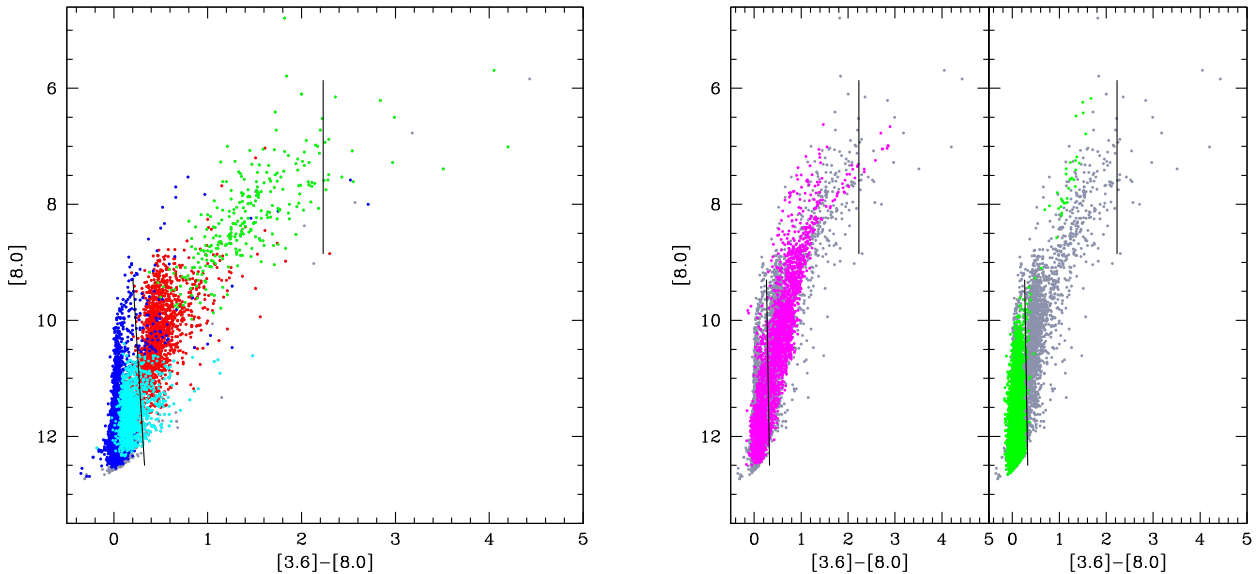


**Figure 10.** Left: the distribution on the colour–magnitude ( $[3.6] - [8.0]$ ,  $[8.0]$ ) plane of the AGB sample of the SMC by Boyer et al. (2011), divided among oxygen-rich stars (blue points), aO-AGB (cyan), carbon stars (red) and X-AGB (green). Right: the results from our synthetic modelling in the same plane, overlaid to the observations by Boyer et al. (2011), shown with light, grey points. The simulated AGB population is divided among oxygen-rich (right side, green points) and carbon-rich AGB stars (left side, magenta).

region II, were classified as oxygen-rich. We interpret these objects as descendants of stars of mass  $\sim 4\text{--}5.5 M_{\odot}$  that have just started to experience HBB, in the phase when the evolutionary tracks move towards region IV of the CCD (see Fig. 3)

The identification of stars in region IV of the CCD with AGB stars experiencing HBB can be tested through spectroscopic analysis: their surface chemical composition would show the signature of HBB, with a C/O ratio below 0.05 and  $^{12}\text{C}/^{13}\text{C}$  close to the equilibrium value,  $\sim 3.3$ . Both these quantities can provide important information on the strength of HBB experienced by massive AGB stars of metallicity  $Z = 8 \times 10^{-3}$  (Ventura et al. 2015).

For what concerns the dust in their surroundings, stars in this region of the CCD are surrounded by alumina dust particles of size  $\sim 0.07 \mu\text{m}$  and silicate grains of dimension  $\sim 0.1 \mu\text{m}$ ; the latter particles give the dominant contribution to the degree of obscuration of these stars, with optical depths in the range  $0.2 < \tau_{10} < 0.8$ .

## 6 A COMPARISON WITH THE ANALYSIS BY BOYER ET AL. (2011)

Boyer et al. (2011) divided the sample of SMC stars according to the schematisation described in Section 2. The AGB stars in their sample were classified as C-rich, O-rich, X-AGB and ‘aO-AGB’ stars. The authors defined the latter group based on the position in the  $J - [8]$  plane (see section 3.1.5 in Boyer et al. 2011), where they can be distinguished from C-rich and O-rich AGB stars.

In the comparison among the number of stars in the various classes, the largest group of objects,  $\sim 43$  per cent of the overall population, fall in the oxygen-rich sample; an additional 21.5 per cent are classified as aO-AGB stars. The remaining AGB stars are divided among carbon stars ( $\sim 30$  per cent) and X-AGB (6 per cent).

In the left-hand panel of Fig. 10 we show the observations by Boyer et al. (2011), in the colour–magnitude  $[3.6] - [8.0]$ ,  $[8.0]$  plane, divided among the aforementioned groups. In the right-hand panel, we show the results from our modelling, overlaid to the observed locii: the objects which we classify as carbon stars are shown on the left, whereas oxygen-rich stars are shown on the right.

First, we find that almost the entire X-AGB sample is composed of carbon stars; only a few objects classified as X-AGB, populating the brighter region of the CMD, can be interpreted as the progeny of massive AGB stars, experiencing HBB.

In the comparison among the results from our simulations, shown in the right side of Fig. 10, and the classification introduced by Boyer et al. (2011) (left-hand panel), we see that part of the stars which we interpret as carbon stars overlap with the aO-AGB sample and, in minor extent, with the O-rich group.

According to our analysis the aO-AGB group introduced by Boyer et al. (2011) is composed of low-mass stars approaching or at the beginning of the C-rich stage. Note that in a very recent work, Boyer et al. (2015), on the basis of optical spectra analysis, claim that 50 per cent of the aO-AGB stars in the SMC are C-rich stars, in agreement with our interpretation. This leads to a slight difference in the relative distribution of oxygen-rich AGB and carbon stars. According to Boyer et al. (2011), carbon stars accounts for  $\sim 36$  per cent of the overall population (based on the previous point, here we added the carbon stars and the X-AGB), whereas according to our interpretation C-stars are  $\sim 46$  per cent of the AGB population of the SMC in the sample by Boyer et al. (2011).

This difference is the reason for the different LF of carbon stars between this study and the results from Boyer et al. (2011). Fig. 11 shows that we predict a higher number of faint C-stars in comparison with Boyer et al. (2011). When the same criterion to separate C-stars from oxygen-rich AGB stars used by Boyer et al. (2011) is adopted, the two results become very similar. Note that on the basis of the new results by Boyer et al. (2015) quoted above, these differences would be significantly reduced.

## 7 THE AGB POPULATIONS IN THE LMC AND SMC

The SAGE-LMC and SAGE-SMC surveys allowed a complete census of the AGB stars in the LMC and SMC. Hundreds of thousands of photometric data were used to produce colour–colour and

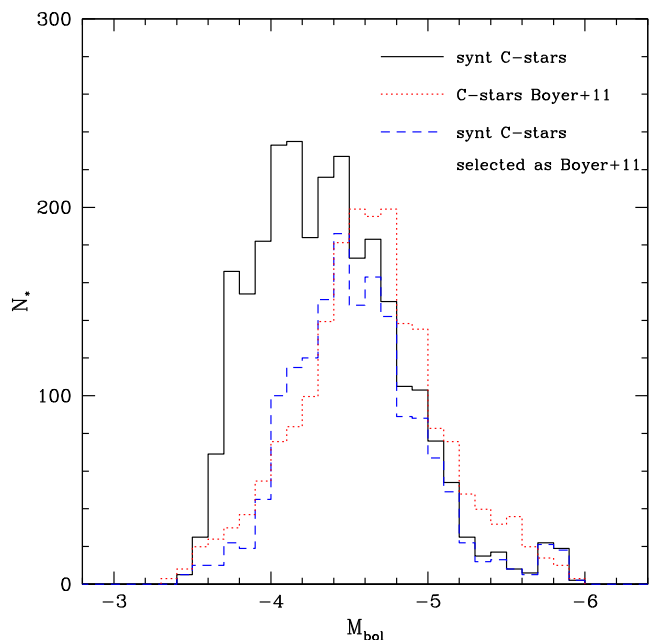


**Figure 11.** The LF of C-stars in the SMC found in this work (black solid track) and in the investigation by Boyer et al. (2011) (red dotted). The blue dashed line is the LF obtained with our models, when the same criterion used by Boyer et al. (2011) to separate C-stars from oxygen-rich objects is adopted.

colour–magnitude diagrams, that can be compared with results from theoretical modelling, with the aim to characterize the sources observed.

The comparison among the infrared colours and magnitudes of the AGB stars in the LMC and SMC shows some similarities but also significant differences, such as the number of AGB stars in the two samples and the distribution of the stars observed among the various groups of the classifications introduced.

D15 focused on the AGB stars in the LMC with the largest infrared emission, called ‘extreme’ (Riebel et al. 2010, 2012); these stars were shown to give the largest contribution to the dust production rate of the LMC. One of the main findings of D15 was that this sample of extreme AGB stars was mainly ( $\sim 95$  per cent) composed of C-rich stars, whereas oxygen-rich AGB give a  $\sim 5$  per cent contribution. This interpretation was in agreement with the conclusions by Riebel et al. (2012), based on GRAMS models. C-stars in the extreme sample (the OCS and EOCS classes introduced in D15) were identified as low-mass stars, whose surface chemistry has been significantly increased in carbon; the oxygen-rich, extreme stars were interpreted as stars experiencing HBB (HBBS in D15).

In the analysis of the X-AGB population of the SMC, presented in Section 5, we also find evidence of carbon-enriched objects and of stars experiencing HBB. However, the comparison with the LMC outlines two important differences.

First, by confronting Fig. 6 with fig. 11 in D15, we note that the sequence of carbon stars in the CCD, discussed in Section 5.2, is much shorter in the SMC: while in the LMC it extends to  $[3.6] - [4.5] \sim 3$ , here we have  $[3.6] - [4.5] < 1.5$ . The reason is the different progenitors of the C-rich AGB stars evolving to the reddest infrared colours in the two galaxies. D15 proposed that the EOCS sample, i.e. the carbon stars in the LMC with the largest infrared emission, descend from stars of metallicity  $Z = 8 \times 10^{-3}$  and initial mass  $M \sim 2.5\text{--}3 M_{\odot}$ . These stars formed during the burst in the SFR of the LMC, which occurred  $\sim 500$  Myr ago (Harris & Zaritsky 2009).

The SFR of the SMC (see Fig. 1) presents a much narrower peak at those ages, with practically no possibility to find stars within this range of mass in such an advanced and short evolutionary phase; consequently, the population of the most obscured C-stars in the SMC descend from stars of initial mass  $\sim 1.5\text{--}1.7 M_{\odot}$  and metallicity  $Z = 4 \times 10^{-3}$ , formed 1–1.5 Gyr ago, during the much longer, secondary peak in the SFR. The comparison between the evolutionary tracks of the  $1.5 M_{\odot}$  model of  $Z = 4 \times 10^{-3}$  (middle panel of Fig. 3) and the  $2.5 M_{\odot}$  model of  $Z = 8 \times 10^{-3}$  (right-hand panel of Fig. 3) shows that the latter evolves to much redder colours, which is the reason for the difference in the extension of the C-star sequence in the observed CCD of the LMC and SMC. On the evolutionary side, as discussed in Section 4.3, this difference is entirely due to the larger amount of carbon accumulated at the surface of the  $2.5 M_{\odot}$  model, as a consequence of the higher number of TDUs experienced. The values reached by the optical depth in the final AGB phases of these models is a further evidence of this behaviour: we have  $\tau_{10} \sim 3$  for  $(M, Z) = (2.5 M_{\odot}, 8 \times 10^{-3})$  and  $\tau_{10} \sim 0.8$  for  $(M, Z) = (1.5 M_{\odot}, 4 \times 10^{-3})$  (see middle and right-hand panels of Fig. 2).

Turning to the oxygen-rich AGB stars, the sample of obscured stars in the SMC, discussed in Section 5.3, includes a much smaller number of objects in comparison to the LMC. In this work we find that the whole sample of X-AGB is almost entirely composed of carbon stars, with a very modest contribution from O-rich sources: Fig. 6 shows that the number of stars populating region IV in the CCD, where O-rich AGB stars evolve during the HBB phase (see Section 5.3), is much smaller than in regions II and III, populated by carbon stars (see Section 5.2). The comparison of the SFH of the two galaxies provides an explanation for this dissimilarity. According to D15, the stars belonging to the HBBS group of the LMC formed  $\sim 100$  Myr ago, during a peak in the SFR of the LMC (Harris & Zaritsky 2009). Looking at Fig. 1, we note that the shape of the SFR of the SMC during the period 50–200 Myr ago is completely different: at odds with the LMC, the SFR of the SMC presents a minimum in that period: a much smaller number of stars formed in that epoch, which motivates the paucity of AGB stars in region IV of the CCD.

The arguments presented here outline that the LMC is a much more favourable environment to investigate dust production by stars evolving through the AGB phase. The LMC, compared to the SMC, harbour a higher percentage of dust-enshrouded AGB stars with a large infrared emission; this holds for oxygen-rich objects and carbon stars. In the first case, the difference among the two galaxies is in the number of stars detected, whereas for dusty C-rich AGB stars we also find a qualitative dissimilarity, in the infrared colours of the most obscured sources, which are significantly redder in the LMC.

The peculiar evolution of the SFR of the LMC is the reason for the presence of such a large percentage of highly obscured AGB stars in this galaxy. This is because the SFR peaks in the two epochs ( $\sim 100$  Myr and  $\sim 500$  Myr ago) when, based on our models of dusty AGB stars, the objects with the highest degree of obscuration formed.

100 Myr is the evolution time of  $\sim 5\text{--}6 M_{\odot}$  stars: this is the range of mass of stars experiencing strong HBB (temperature at bottom of the convective envelope  $T > 90$  MK) during the AGB phase, with the formation of large amounts of dust and a high infrared emission. Within the sample of oxygen-rich stars, these are the sources which reach the largest degree of obscuration. Models of higher mass would also evolve to extremely red colours; however, a very few stars in this range of mass are expected, for reasons associated with

the mass function and the short duration of the AGB phase of stars in this mass range.

An earlier episode of strong star formation took place in the LMC  $\sim 500$  Myr ago. This is the formation epoch of  $Z = 8 \times 10^{-3}$  stars of mass in the range  $2.5\text{--}3 M_{\odot}$ . Among all the stars evolving through the C-star phase, these are the stars experiencing the highest number of TDU episodes, thus accumulating the largest quantities of carbon in the surface regions: the winds of these stars are therefore an extremely favourable environment for the formation of carbonaceous solid particles, which explains their extremely red infrared colours. Fig. 3 shows that the evolutionary tracks of stars in this range of mass, and metallicity  $Z = 4, 8 \times 10^{-3}$ , are those reaching the reddest infrared colours during the final phases of the evolution as carbon stars.

## 8 CONCLUSIONS

We study the population of AGB stars of the SMC. Our analysis is based on the comparison between *Spitzer* observations and theoretical modelling of the AGB phase. The description of the AGB evolution relies on a full integration of the equations of stellar structure and on the description of the dust formation process in the circumstellar envelope; accounting for the presence of dust is crucial to interpret the *Spitzer* colours of the most obscured AGB stars, the sources with the largest infrared emission.

In the colour–colour ( $[3.6] - [4.5]$ ,  $[5.8] - [8.0]$ ) diagram and in the colour–magnitude ( $[3.6] - [8.0]$ ,  $[8.0]$ ) plane, we distinguish a population of stars with negligible infrared emission, composed mainly of oxygen-rich, low-mass stars of various metallicity, in the AGB phases previous to the C-star phase; this region of the CCD is also populated by some carbon stars with a small degree of obscuration, either in the early phases after the achievement of the C-star stage, or in the phases following each thermal pulse, before hydrogen burning in the shell is fully restored.

The sequences of dusty AGB stars with infrared emission bifurcate in the colour–colour plane. Carbon stars trace a diagonal band, the reddest objects having  $[3.6] - [4.5] \sim 1.5$ ,  $[5.8] - [8.0] \sim 1$ . We interpret this population of C-rich objects as an obscuration sequence: the reddest sources correspond to the stars that experienced the largest number of Third Dredge-Up episodes, with a higher content of carbon in the surface zones. The SED of these AGB stars exhibits a large infrared emission, owing to the effects of the large quantities of carbonaceous dust, formed in their winds. The carbon star sample in the SMC descend from stars of mass  $1.5\text{--}2 M_{\odot}$  and metallicity  $Z = 4 \times 10^{-3}$ , formed between 700 Myr and 2 Gyr ago, and from a few Gyr old population of lower metallicity objects, of mass below  $1.5 M_{\odot}$ . The C-rich objects of the SMC with the largest degree of obscuration descend from stars of initial mass  $\sim 1.5\text{--}1.7 M_{\odot}$  and metallicity  $Z = 4 \times 10^{-3}$ , formed  $\sim 3$  Gyr ago, during the secondary peak in the SFR of the SMC.

The oxygen-rich AGB stars, surrounded by dust, populate regions in the colour–colour plane uncovered by the carbon rich sample. This is due to the prominent silicate feature at  $9.7 \mu\text{m}$ , in the SED, which provokes a higher flux in the  $[8.0]$  flux, for a given degree of obscuration. The oxygen-rich stars with the largest infrared emission are interpreted as the progeny of massive AGB stars of initial mass  $\sim 5\text{--}6 M_{\odot}$  and metallicity  $Z = 8 \times 10^{-3}$ , experiencing HBB; these stars formed  $\sim 100$  Myr ago.

The comparison among the sample of obscured AGB stars in the SMC and LMC, called ‘extreme’, outlines two important differences: (a) while oxygen-rich AGB stars in the LMC account for  $\sim 5$  per cent of the total sample, their contribution in the SMC

is much smaller; (b) the observed sequence of the obscured carbon stars in the CCD of the LMC extends to  $[3.6] - [4.5] \sim 3$ , whereas the population of C-rich objects in the SMC is included in the region  $[3.6] - [4.5] < 1.5$ .

Both these evidences indicate that dust production by AGB stars is much higher in the LMC than in the SMC. This is motivated by the different SFH of the two galaxies. The evolution with time of the SFR of the LMC proves extremely favourable to dust production by AGB stars. This originates from the two peaks at  $\sim 100$  Myr and  $\sim 500$  Myr. These are the evolution times of the sources producing the larger quantities of dust, namely the stars of mass  $\sim 5\text{--}6 M_{\odot}$ , producing considerable quantities of silicates, and those with mass  $\sim 2.5\text{--}3 M_{\odot}$ , which provide the largest contribution to production of carbonaceous particles.

## ACKNOWLEDGEMENTS

The authors are indebted to the anonymous referee for the careful reading of the manuscript and for the detailed and relevant comments that helped to increase the quality of this work. FD thanks F. Kemper for making available the spectroscopically confirmed sample and Martha Boyer for useful indications concerning photometrical uncertainties. PV was supported by PRIN MIUR 2011 ‘The Chemical and Dynamical Evolution of the Milky Way and Local Group Galaxies’ (PI: F. Matteucci), prot. 2010LY5N2T. DAGH acknowledges support provided by the Spanish Ministry of Economy and Competitiveness under grant AYA2014-58082-P. RS acknowledges funding from the European Research Council under the European Unions Seventh Framework Programme (FP/2007-2013)/ERC Grant Agreement no. 306476. MDC acknowledges support from the Observatory of Rome.

## REFERENCES

- Aringer B., Girardi L., Nowotny W., Marigo P., Lederer M. T., 2009, *A&A*, 503, 913
- Bertoldi F. et al., 2003, *A&A*, 409, L47
- Bianchi S, Schneider R., 2007, *MNRAS*, 378, 973
- Blöcker T., 1995, *A&A*, 297, 727
- Bolatto A. D. et al., 2007, *ApJ*, 655, 212
- Bowen G. H., 1988, *ApJ*, 329, 299
- Boyer M. L. et al., 2011, *AJ*, 142, 103
- Boyer M. L. et al., 2015, *ApJ*, 810, 116
- Calura F., Pipino A., Matteucci F., 2008, *A&A*, 479, 669
- Cameron A. G. W., Fowler W. A., 1971, *ApJ*, 164, 111
- Canuto V. M., 1992, *ApJ*, 392, 218
- Canuto V. M., 1993, *ApJ*, 416, 331
- Canuto V. M. C., Mazzitelli I., 1991, *ApJ*, 370, 295
- Cioni M.-R. L., van der Marel R. P., Loup C., Habing H. J., 2000, *A&A*, 359, 601
- Cioni M. R. L., Girardi L., Marigo P., Habing H. J., 2006a, *A&A*, 448, 77
- Cioni M. R. L., Girardi L., Marigo P., Habing H. J., 2006b, *A&A*, 452, 195
- Cloutmann L., Eoll J. G., 1976, *ApJ*, 206, 548
- De Bannassuti M., Schneider R., Valiante R., Salvadori S., 2014, *MNRAS*, 445, 3039
- Dell’Agli F., García-Hernández D. A., Rossi C., Ventura P., Di Criscienzo M., Schneider R., 2014a, *MNRAS*, 441, 1115
- Dell’Agli F., Ventura P., García-Hernández D. A., Schneider R., Di Criscienzo M., Brocato E., D’Antona F., Rossi C., 2014b, *MNRAS*, 442, L38
- Dell’Agli F., Ventura P., Schneider R., Di Criscienzo M., García-Hernández D. A., Rossi C., Brocato E., 2015, *MNRAS*, 447, 2992 (D15)
- Di Criscienzo M. et al., 2013, *MNRAS*, 433, 313

- Doherty C. L., Gil-Pons P., Lau H. B., Lattanzio J. C., Siess L., 2014, *MNRAS*, 437, 195
- Dwek E., 1998, *ApJ*, 501, 643
- Ferrarotti A. D., Gail H. P., 2001, *A&A*, 371, 133
- Ferrarotti A. D., Gail H. P., 2002, *A&A*, 382, 256
- Ferrarotti A. D., Gail H. P., 2006, *A&A*, 553, 576
- Gail H. P., Sedlmayr E., 1985, *A&A*, 148, 183
- Gail H. P., Sedlmayr E., 1999, *A&A*, 347, 594
- García-Hernández D. A., García-Lario P., Plez B., D'Antona F., Manchado A., Trigo-Rodríguez J. M., 2006, *Science*, 314, 1751
- García-Hernández D. A., García-Lario P., Plez B., Manchado A., D'Antona F., Lub J., Habing H., 2007, *A&A*, 462, 711
- García-Hernández D. A. et al., 2009, *ApJ* 705, L31
- Gehrz R. D., 1989, in L. J., Tielens A. G. G. M., eds, *Proc. IAU Symp.* 135, *Interstellar Dust*. Kluwer, Dordrecht, p. 445
- Gordon K. D. et al., 2011, *AJ*, 142, 102
- Grevesse N., Sauval A. J., 1998, *Space Sci. Rev.*, 85, 161
- Hanner M., 1988, Technical report, *Grain Optical Properties*.
- Harris J., Zaritsky D., 2004, *AJ*, 127, 1531
- Harris J., Zaritsky D., 2009, *ApJ*, 138, 1243
- Hauschildt P. H., Allard F., Ferguson J., Baron E., Alexander D. R., 1999, *ApJ*, 525, 871
- Ita Y. et al., 2010, *PASJ*, 62, 273
- Keller S. C., Wood P. R., 2006, *ApJ*, 642, 834
- Koike C., Kaito C., Yamamoto T., Shibai H., Kimura S., Suto H., 1995, *Icarus*, 114, 203
- Maiolino R., Schneider R., Oliva E., Bianchi S., Ferrara A., Mannucci F., Pedani M., Roca Sogorb M., 2004, *Nature*, 431, 533
- Marigo P., 2002, *A&A*, 387, 507
- Marigo P., Aringer B., 2009, *A&A*, 508, 1538
- Mazzitelli I., 1989, *ApJ*, 340, 249
- Mazzitelli I., D'Antona F., Ventura P., 1999, *A&A*, 348, 846
- Meixner M. et al., 2006, *AJ*, 132, 2268
- Miville-Deschenes M.-A., Lagache G., 2005, *ApJS*, 157, 302
- Nanni A., Bressan A., Marigo P., Girardi L., 2013a, *MNRAS*, 434, 488
- Nanni A., Bressan A., Marigo P., Girardi L., 2013b, *MNRAS*, 434, 2390
- Nanni A., Bressan A., Marigo P., Girardi L., 2014, *MNRAS*, 438, 2328
- Nenkova M., Ivezić Z., Elitzur M., 1999, in Sprague A., Lynch D. K., Sitko M., eds, *LPI Contributions 969, Workshop on Thermal Emission Spectroscopy and Analysis of Dust, Disks, and Regoliths*. Lunar and Planetary Institute, Houston, TX, p. 20
- Ordal M. A., Bell R. J., Alexander R. W., Newquist L. A., Querry M. R., 1988, *Appl. Opt.*, 27, 1203
- Ossenkopf V., Henning T., Mathis J. S., 1992, *A&A*, 261, 567
- Pegourie B., 1988, *A&A*, 194, 335
- Pipino A., Fan X. L., Matteucci F., Calura F., Silva L., Granato G., Maiolino R., 2011, *A&A*, 525, A61
- Plez B., Smith V. V. S., Lambert D. L., 1993, *ApJ*, 418, 812
- Price S. D., Egan M. P., Carey S. J., Mizuno D. R., Kuchar T. A., 2001, *AJ*, 121, 2819
- Riebel D., Meixner M., Fraser O., Srinivasan S., Cook K., Vijn U., 2010, *ApJ*, 723, 1195
- Riebel D., Srinivasan S., Sargent B., Meixner M., 2012, *ApJ*, 753, 71
- Ruffle P. M. E. et al., 2015, *A&A*, *MNRAS*, 451, 3504
- Sackmam I. J., Boothroyd A. I., 1992, *ApJ*, 392, L71
- Schneider R., Valiante R., Ventura P., Dell'Agli F., Di Criscienzo M., Hirashita H., Kemper F., 2014, *MNRAS*, 442, 1440
- Schweiring P. B. W., Israel F. P., 1989, *A&AS*, 79, 79
- Smith V. V., Plez B., Lambert D., 1995, *AJ*, 441, 735
- Srinivasan S., Sargent B. A., Meixner M., 2011, *A&A*, 532, A54
- Valiante R., Schneider R., Bianchi S., Andersen A., Anja C., 2009, *MNRAS*, 397, 1661
- Valiante R., Schneider R., Salvadori S., Bianchi S., 2011, *MNRAS*, 416, 1916
- Ventura P., D'Antona F., 2005a, *A&A*, 431, 279
- Ventura P., D'Antona F., 2005b, *A&A*, 439, 1075
- Ventura P., D'Antona F., 2009, *MNRAS*, 499, 835
- Ventura P., D'Antona F., 2011, *MNRAS*, 410, 2760
- Ventura P., Marigo P., 2009, *MNRAS*, 399, L54
- Ventura P., Marigo P., 2010, *MNRAS*, 408, 2476
- Ventura P., Zepieri A., Mazzitelli I., D'Antona F., 1998, *A&A*, 334, 953
- Ventura P. et al., 2012a, *MNRAS*, 420, 1442
- Ventura P. et al., 2012b, *MNRAS*, 424, 2345
- Ventura P., Di Criscienzo M., Carini R., D'Antona F., 2013, *MNRAS*, 431, 3642
- Ventura P., Di Criscienzo M., D'Antona F., Vesperini E., Tailo M., Dell'Agli F., D'Ercole A., 2014a, *MNRAS*, 437, 3274
- Ventura P., Dell'Agli F., Di Criscienzo M., Schneider R., Rossi C., La Franca F., Gallerani S., Valiante R., 2014b, *MNRAS*, 439, 977
- Ventura P., Karakas A. I., Dell'Agli F., Boyer M. L., García-Hernández D. A., Di Criscienzo M., Schneider R., 2015, *MNRAS*, 450, 3181
- Wachter A., Schröder K. P., Winters J. M., Arndt T. U., Sedlmayr E., 2002, *A&A*, 384, 452
- Wachter A., Winters J. M., Schröder K. P., Sedlmayr E., 2008, *A&A*, 486, 497
- Wang R. et al., 2008, *ApJ*, 687, 848
- Wang R., Wagg J., Carilli C. L., Walter F., Lentati L., Fan X., Riechers D. A., Bertoldi F., 2013, *ApJ*, 773, 44
- Westerlund B. E., 1997, *The Magellanic Clouds*. Cambridge Univ. Press, Cambridge
- Wilke K., Stickel M., Haas M., Herbstmeier U., Klaas U., Lemke D., 2003, *A&A*, 401, 873

This paper has been typeset from a  $\text{\TeX}/\text{\LaTeX}$  file prepared by the author.